J. Fluid Mech. (2010), *vol.* 644, *pp.* 473–507.
doi:10.1017/S0022112009992618

Shock regularization in dense gases by viscous–inviscid interactions

A. KLUWICK† AND G. MEYER

Institute of Fluid Mechanics and Heat Transfer, Vienna University of Technology, Resselgasse 3/322, 1040 Vienna, Austria

(Received 26 May 2009; revised 6 October 2009; accepted 6 October 2009)

Transonic high-Reynolds-number flows through channels which are so narrow that the classical boundary-layer approach fails locally are considered in the presence of a weak stationary normal shock. As a consequence, the properties of the inviscid core and the viscosity-dominated boundary-layer region can no longer be determined in subsequent steps but have to be calculated simultaneously in a small interaction region. Under the requirement that the core-region flow should be considered to be one-dimensional to the leading order the resulting problem of shock–boundary-layer interaction is formulated by the means of matched asymptotic expansions for laminar flows of dense gases (Bethe–Zel'dovich–Thompson, or BZT, fluids). Such fluids have the distinguishing feature that the fundamental derivative of gas dynamics can become negative or even change sign under the thermodynamic conditions to be considered. The regularizing properties of the mechanism of viscous–inviscid interactions on the different anomalous shock forms possible in the flow of dense gases with mixed nonlinearity, namely rarefaction, sonic, double-sonic and split shocks, will be discussed. To this end we show the consistency of the resulting internal-shock profiles because of strong shock–boundary-layer interaction with a generalized shock admissibility criterion formulated for the case of purely inviscid flows. Representative solutions for the internal-shock structures are presented, and the importance of such flow phenomena in technical applications in the near future are shortly discussed by considering estimates of the actual dimensions of the interaction region for a specific representative situation in which the BZT fluid PP10 ($C_{13}F_{22}$) has been selected.

1. Introduction

After an era of vivid interest in dense gases that are also known as Bethe–Zel'dovich–Thompson (BZT) fluids, starting with the works of Bethe (1942), Zel'dovich (1946) and Thompson (1971) and lasting until the middle of 1990s (cf. amongst others Thompson & Lambrakis 1973; Cramer & Kluwick 1984; Cramer & Sen 1986; Thompson *et al.* 1987; Cramer 1989; Chandrasekar & Prasad 1991; Cramer & Crickenberger 1991; Kluwick 1993, 1994; Kluwick & Scheichl 1996), there has been a renewed interest in these kind of fluids as can be observed by the number of more recent publications dealing with the experimental prediction and detection of anomalous shocks inherent to these kind of fluids (Fergason *et al.* 2001; Colonna &

† Email address for correspondence: alfred.kluwick@tuwien.ac.at

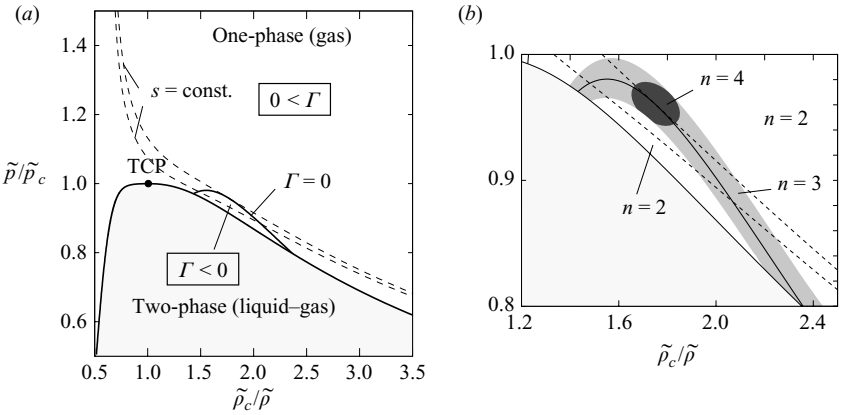

FIGURE 1. (*a*) Pressure versus density diagram for a BZT fluid (PP10, according to the Martin–Hou equation of state; cf. § 5.2). The subscript c indicates thermodynamic quantities evaluated at the critical thermodynamical point TCP. (*b*) Close-up of the region of negative Γ and subdivision in regions with the asymptotic properties: $\Gamma \sim 1$, $\Gamma \gtrless 0$ $(n=2)$; $|\Gamma| \ll 1$, $(\partial\Gamma/\partial\rho)_s \sim 1$ $(n=3)$; and $|\Gamma| \ll 1$, $|(\partial\Gamma/\partial\rho)_s| \ll 1$, $(\partial^2\Gamma/\partial\rho^2)_s \sim 1$ $(n=4)$.

Silva 2003; Guardone & Argrow 2005; Colonna & Guardone 2006; Zamfirescu, Guardone & Colonna 2008), given their possible technical applications in thermal turbomachinery (see e.g. Cinnella & Congedo 2007; Colonna, Guardone & Nannan 2007).

A distinguishing property of dense gases is that these exhibit thermodynamic regions of negative or mixed nonlinearity in the single-phase state, by which is meant that the so-called fundamental derivative

$$\Gamma = \frac{1}{\tilde{c}} \frac{\partial(\tilde{\rho}\tilde{c})}{\partial\tilde{\rho}}\bigg|_{\tilde{s}} \tag{1.1}$$

takes on negative values or even changes sign in the flow field, respectively. This feature, which, however, is restricted to a small region in the vicinity of the thermodynamical critical point (cf. figure 1*a*), has severe consequences for the theory of compressible inviscid flows, giving rise to a rich variety of anomalous shock forms which are not possible in the common case of Γ being strictly positive, as there are rarefaction, sonic, double-sonic and split shocks (cf. Kluwick 1993). Here $\tilde{c}$ is the speed of sound,

$$\tilde{c} = \sqrt{\left(\frac{\partial\tilde{p}}{\partial\tilde{\rho}}\right)_{\tilde{s}}}, \tag{1.2}$$

and $\tilde{p}$, $\tilde{\rho}$ and $\tilde{s}$ are the pressure, the density and the entropy, respectively. Most important of all, the classical criteria, such as the requirement that the thermodynamic entropy has to increase over a shock following from the second law of thermodynamics or the more mathematical condition for the stability of the resulting wave pattern expressed by Lax's characteristic criterion (Menikoff & Plohr 1989) or by the more general Oleinik condition (Oleinik 1957; Kluwick, Scheichl & Cox 2007), are too weak to rule out inadmissible shocks in case of fluids exhibiting mixed nonlinearity. A shock is considered inadmissible in this context if there exists no internal-shock profile connecting the flow conditions before and after the shock when physical effects that have been neglected so far are taken into account and thus regularize

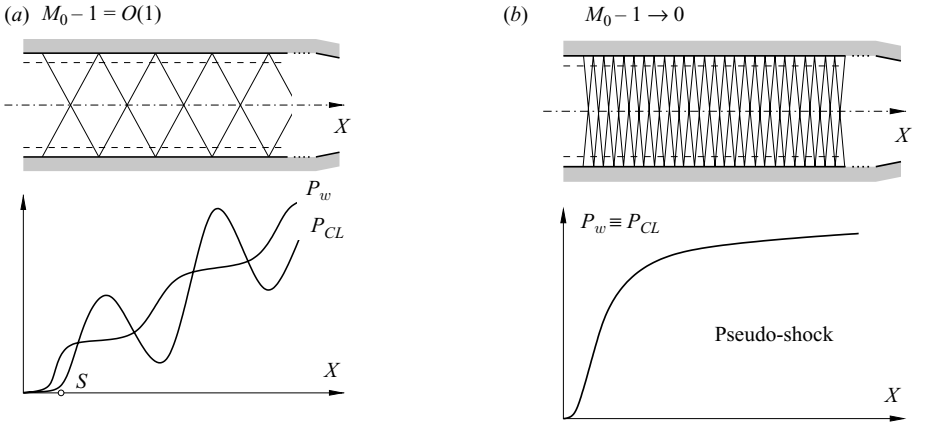

FIGURE 2. Schematic representation of freely interacting channel flow: —, wave fronts; ---, boundary layers; P_w, wall pressure; P_{CL}, pressure at channel centreline; M_0, Mach number at reference state; S, separation point. (a) Purely supersonic flow: $M_0 - 1 = O(1)$. (b) Transonic flow: $M_0 - 1 \ll 1$.

the problem. It is commonly known that the consideration of small effects of viscosity and heat conduction in the vicinity of the shock front leads to such smooth internal-shock profiles; for a thorough discussion of thermo-viscous regularization for fluids exhibiting mixed nonlinearity, see e.g. Cramer & Kluwick (1984), Cramer & Crickenberger (1991) or Kluwick (1993).

In the present paper quite a different mechanism for the regularization of weak shocks is proposed, which is based on shock–boundary-layer interaction taking place in transonic high-Reynolds-number flows through narrow channels. The situation to be described here is closely related to the pseudo-shock phenomenon encountered in internal gas flows (Matsuo, Miyazato & Kim 1999). A heuristic explanation for the proclaimed regularizing influence of strong shock–boundary-layer interaction is given in figure 2. Figure 2(a) is a sketch of the numerical results obtained by Kluwick & Bodonyi (1979) for purely supersonic internal interacting flows. If the governing equations for the core-region flow are linear (weak shocks), then an oblique compression shock is reflected at the free edge of the boundary layer at the wall as a rarefaction discontinuity (being the linear counterpart to a Prandtl–Meyer expansion fan that forms if nonlinear effects are accounted for) and vice versa. Considering the pressure distribution along the centreline of the channel one finds distinct pressure oscillations but a net pressure rise over the length of the 'shock train'. The pressure distribution at the channel wall, however, is monotonously increasing as a result of the shock–boundary-layer interaction exhibiting a plateau region where the compression shock impinges on the boundary layer and is reflected as a rarefaction discontinuity. If sonic flow conditions are approached (cf. figure 2b), that is to say taking the limit $M_0 \to 1+$, the number of reflections per length is increasing, eventually leading to the situation in which the flow in the core region becomes one-dimensional, and the pressure distribution along the centreline and along the walls collapse, forming a smooth pseudo-shock.

To be specific, the resulting shock–boundary-layer interaction problem shall be formulated for transonic internal dense-gas flows by means of matched asymptotic expansions exploiting the largeness of the Reynolds number and the asymptotic

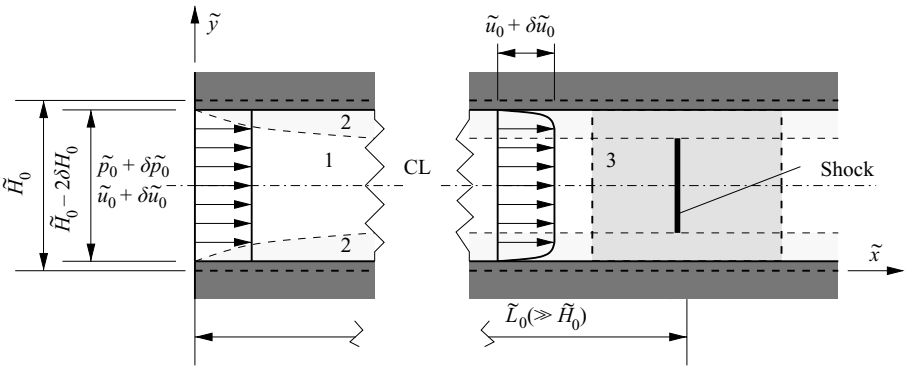

FIGURE 3. Schematic sketch of the problem set-up: region 1, inviscid core; region 2, viscous non-interacting boundary layers; region 3, viscous–inviscid interaction.'CL' stands for centreline.

properties of the fundamental derivative depicted in figure 1(*b*). To this end, consider the situation of a stationary weak normal shock in a narrow channel depicted in figure 3. Near the channel inlet viscous effects at high Reynolds numbers are limited to thin layers adjacent to the channel walls, and in general, Prandtl's classical boundary-layer theory for laminar flow can be applied with good accuracy (except for a tiny region near the leading edge, where the full Navier–Stokes equations apply as in the case of external flows). However, rapid changes in the streamwise flow field, such as evoked by a weak normal shock, lead to a local breakdown of the classical boundary-layer approach (cf. Stewartson 1974 or Kluwick 1998, amongst others). As a direct consequence, the properties of the inviscid core and the viscosity-dominated boundary-layer regions can no longer be determined in subsequent steps but have to be calculated simultaneously within an asymptotically small interaction region around the shock depicted by region 3 in figure 3. The interaction problem can be described consistently by a triple-deck problem (cf. Stewartson 1974), where the inviscid interacting core region is represented by a single upper deck which is shared by the two interacting boundary layers at the lower and upper channel walls. The interacting boundary layer itself subdivides into an asymptotically thin lower deck accounting for near-wall effects of viscosity and a passive main deck comprising the main part of the interacting boundary layer. The channel shall be sufficiently narrow so that the flow in the inviscid core becomes one-dimensional to the leading order. As a consequence, the present work can be seen as an addition to the one-dimensional weak normal shock theory for inviscid internal flows of dense gases through nozzles, outlined in Kluwick (1993). The paper is dedicated to the discussion of stationary internal-weak-shock profiles; however, for a discussion of the linear spatial stability of distinguished trivial solutions to the problem we will rely on the unsteady formulation of the viscous–inviscid interaction problem. Therefore, unsteady effects are included into the mathematical derivation of the fundamental equations *ab initio*. A discussion of transonic high-Reynolds-number flows through slender nozzles in general and the conversion of subsonic to supersonic flow in particular, where the boundary-layer correction can no longer be considered to be an effect of the higher order, will be published in a forthcoming second part by the authors.

The paper at hand is structured as follows. Suitable reference states for the various quantities imminent to the problem set-up and the governing equations in dimensionless form are introduced in § 2, followed by a discussion of the magnitude

of the various dimensionless groups entering the equations (§ 2.1). The asymptotic analysis which eventually yields the fundamental (lower-deck) problem describing the interacting flow regime in the channel is presented in § 3. In § 3.3 we present a brief discussion of links to the purely inviscid theory given by Kluwick (1993). Finally, internal-shock profiles of compression, rarefaction, sonic, double-sonic and split shocks are discussed with respect to inviscid shock theory. In § 4 the asymptotic properties of internal-shock profiles are analysed analytically, and in § 5 representative numerical solutions for a selected example of BZT fluid, PP10 ($C_{13}F_{22}$), are presented. Most important of all, calculations of the characteristic length scales imminent to the problem in case of the working fluid PP10 in § 5.2 give an impression of the actual size of technical flow devices, where the phenomena described in this paper are expected to be encountered in dense-gas flows.

2. Problem formulation I – governing equations

The non-dimensional quantities are introduced as follows, with the tilde denoting the dimensional quantities:

$$(\tilde{x},\tilde{y})=\tilde{L}_0(x,y),\quad \tilde{H}_0=\tilde{L}_0H_0,\quad (\tilde{u},\tilde{v})=\tilde{u}_0(u,v),\quad \tilde{t}=\frac{\tilde{L}_0}{\tilde{u}_0}\,t,\quad \tilde{c}=\tilde{c}_0\,c,$$
$$\tilde{\rho}=\tilde{\rho}_0\,\rho,\quad \tilde{p}=\tilde{\rho}_0\tilde{u}_0^2\,p,\quad \tilde{\theta}=\tilde{\theta}_0\,\theta,\quad \tilde{h}=\tilde{u}_0^2\,h,\quad \tilde{s}=\tilde{c}_{p,0}s,$$
$$\tilde{\mu}=\tilde{\mu}_0\,\mu,\quad \tilde{\mu}_b=\tilde{\mu}_0\,\mu_b,\quad \tilde{k}=\tilde{k}_0\,k.$$

Here $(\tilde{x},\tilde{y})$ denote the coordinates in the horizontal and vertical directions and $(\tilde{u},\tilde{v})$ the corresponding components of the velocity vector with $\tilde{t}$ denoting the time, $\tilde{c}$ the speed of sound, $\tilde{\rho}$ the density, $\tilde{p}$ the pressure, $\tilde{\theta}$ the temperature, $\tilde{h}$ the specific enthalpy, $\tilde{s}$ the specific entropy, $\tilde{c}_p$ the specific heat capacity at constant pressure, $\tilde{\mu}$ the dynamic viscosity, $\tilde{\mu}_b$ the bulk viscosity and $\tilde{k}$ the thermal conductivity. The subscript 0 indicates a reference state defined by the flow quantities evaluated in the undisturbed core region immediately upstream of the interaction region at a fixed position $\tilde{L}_0$ for a chosen initial configuration (cf. figure 3); δH_0, δu_0, $\delta\rho_0$ and δp_0 introduced in figure 3 denote small variations of the channel height and the inflow conditions with respect to the chosen reference state.

Then the Navier–Stokes equations for two-dimensional compressible flows neglecting gravitational forces can be written in the following form:

$$\frac{\partial\rho}{\partial t}+\partial_i(\rho u_i)=0, \tag{2.1a}$$

$$\rho\left(\frac{\partial u_i}{\partial t}+u_j\partial_j u_i\right)=-\partial_i p+\frac{1}{Re}\,\partial_j\tau_{ij}, \tag{2.1b}$$

$$\frac{c^2}{M_0^2}\frac{\mathrm{D}\rho}{\mathrm{D}t}-\frac{\mathrm{D}p}{\mathrm{D}t}=\frac{G_0\bar{G}}{Re}\left(\tau_{ij}\partial_j u_i+\frac{1}{Pr\,Ec}\,\partial_k(k\,\partial_k\theta)\right), \tag{2.1c}$$

with the stress tensor for a Newtonian fluid $\tau_{ij}=\mu_b\partial_k u_k\delta_{ij}+\mu(\partial_j u_i+\partial_i u_j-(2/3)\partial_k u_k\delta_{ij})$ and the substantial derivative $\mathrm{D}\bullet/\mathrm{D}t$. Here the dimensionless groups

$$Re:=\frac{\tilde{\rho}_0\tilde{L}_0}{\tilde{\mu}_0},\quad M_0:=\frac{\tilde{u}_0}{\tilde{c}_0},\quad Ec:=\frac{\tilde{u}_0^2}{\tilde{c}_{p,0}\tilde{T}_0},\quad Pr:=\frac{\tilde{k}_0}{\tilde{\mu}_0\tilde{c}_{p,0}},\quad G_0:=\frac{\tilde{\rho}_0}{\tilde{\theta}_0}\left(\frac{\partial\tilde{\theta}}{\partial\tilde{\rho}}\right)_{\tilde{s},0} \tag{2.2}$$

denote the Reynolds, the Mach, the Eckert and the Prandtl number and the Grüneisen coefficient G evaluated at the reference state, respectively; $\bar{G}=G/G_0=O(1)$ denotes a

	Regular fluid	Dense gas
Re	$\gg 1$	$\gg 1$
M_0	≈ 1	≈ 1
Ec	$O(1)$	$\ll 1$
Pr	$O(1)$	$O(1)$
G_0	$O(1)$	$\ll 1$

TABLE 1. Assumptions of the order of magnitude for various dimensionless groups.

properly scaled Grüneisen coefficient. For later convenience we introduce the quantity

$$\bar{c} := c/M_0 = \tilde{c}/\tilde{u}_0. \tag{2.3}$$

The centreline of the nozzle $y = H_0/2$ is a line of symmetry,

$$\frac{\partial u}{\partial y} = \frac{\partial p}{\partial y} = 0, \quad x > 0, \quad y = \frac{H_0}{2}; \tag{2.4}$$

consequently in the following the boundary conditions are specified for the lower half-plane only. The boundary conditions at the (adiabatic) wall are

$$(u, v) = (0, 0), \quad \frac{\partial \theta}{\partial y} = 0, \quad x > 0, \quad y = \delta H_0, \tag{2.5}$$

and those at the channel inflow, i.e. $x = 0$, $\delta H_0 < y < H_0 - \delta H_0$, are

$$(u, v) = (1 + \delta u_0, 0), \quad \rho = 1 + \delta \rho_0, \quad p = p_0 + \delta p_0. \tag{2.6}$$

Unsteady effects will only be considered in a stability analysis, and these shall be restricted to the interaction region, i.e. region 3 in figure 3.

2.1. *Order of magnitude for relevant dimensionless groups*

Table 1 summarizes the assumptions of the orders of magnitude for the dimensionless groups (2.2) which are important for the problem at hand for both regular, that is perfect gas-like, fluids and dense gases. In the following, it will be assumed that $Re \gg 1$ and $M_0 \approx 1$. The first condition leads to the formation of viscosity-dominated boundary layers at the channel walls. The second condition, assumption of transonic flow $M_0 \approx 1$, allows the study of weak shocks causing a transition from supersonic to subsonic flow conditions in the core region of the channel within the framework of an asymptotic theory.

The magnitude of Ec depends on the fluid under consideration. For perfect gas with constant specific heats the relation $Ec = (\gamma - 1)M_0^2 = O(1)$ holds. However, for dense gases one obtains the estimate $Ec = O(M_0^2\ \tilde{R}_g/\tilde{c}_v)$ (cf. Kluwick 1994). Since in case of dense gases the ratio of the specific gas constant $\tilde{R}_g$ and the specific heat at constant volume $\tilde{c}_v$ is small because of the relatively large values of the specific heats in compounds of higher complexity (cf. Kluwick 1994; Colonna & Guardone 2006), $0 < \tilde{R}_g/\tilde{c}_v \ll 1$, this suggests $Ec \to 0$ in the dense-gas limit of $\tilde{R}_g/\tilde{c}_v \to 0$.

Interestingly enough, in both cases the Prandtl number is of order one, $Pr = O(1)$. Whereas this is a well-known and validated fact for a perfect gas it is, in the case of dense gases, only founded on empirical correlations, since measurements in the dense-gas regime are extremely difficult (Kluwick 1994). These have been supported by numerical calculations relying on the method of Chung *et al.* (1988) to calculate the corresponding transport quantities for PP11, $C_{14}F_{24}$ (cf. Kluwick 1994).

Finally, we require that $G_0 = O(1)$ at most. Here the van der Waals equation of state is used as the simplest equation of state which provides a qualitatively correct description of dense-gas behaviour in order to estimate numerical values of G_0 for various reference states located in the single-phase region. It is hereby found that the very close vicinity of the thermodynamical critical point, where G_0 exhibits unbounded growth, has to be excluded from the discussion. However, this restriction is not crucial (in fact it even turns out that $G_0 = O(\tilde{R}_g/\tilde{c}_v)$ for dense gases elsewhere), since the thermodynamic region which is of interest here, i.e. the region in which the fundamental derivative changes its sign, is located sufficiently far away from the thermodynamical critical point (cf. Kluwick 2004; see also figure 1*b*).

2.2. *One-dimensional transonic flow in channel core*

As has been pointed out before, the interacting inviscid flow in the channel core shall be one-dimensional to the leading order. Therefore, the governing equations for one-dimensional compressible flow through channels of variable height, assuming $H = H(x, t)$,

$$\frac{\partial}{\partial t}(\rho H) + \partial_x(\rho u H) = 0, \tag{2.7a}$$

$$\frac{\partial u}{\partial t} + u\partial_x u + \frac{1}{\rho}\partial_x p = O(Re^{-1}), \tag{2.7b}$$

$$\rho\theta\frac{\mathrm{D}s}{\mathrm{D}t} = O(Re^{-1}), \tag{2.7c}$$

are shortly introduced at this point, as these will be used in the inspection analysis to determine the magnitude of the induced perturbations in the core of the interaction region in § 3.1. It is convenient to write the quasi-linear hyperbolic system (2.7*a*)–(2.7*c*) (for $Re \to \infty$) in the form of compatibility conditions along the right and left running characteristics $\mathrm{d}x/\mathrm{d}t = u \pm \bar{c}$:

$$\rho\left(\frac{\partial u}{\partial t} + (u \pm \bar{c})\partial_x u\right) \pm \bar{c}\left(\frac{\partial \rho}{\partial t} + (u \pm \bar{c})\partial_x \rho\right) = \mp\frac{\rho\bar{c}u\partial_x H}{H} \mp \frac{\rho\bar{c}}{H}\frac{\partial H}{\partial t}. \tag{2.8}$$

A shock discontinuity has to satisfy the Rankine–Hugoniot conditions (as has been mentioned before in the 'Introduction', we consider only stationary shock discontinuities)

$$[\rho u] = 0, \tag{2.9a}$$

$$u^a u^b[\rho] = [p], \tag{2.9b}$$

$$2\rho^a\rho^b[h] = (\rho^a + \rho^b)[p], \tag{2.9c}$$

$$[s] \geqslant 0, \tag{2.9d}$$

where the brackets denote jumps, i.e. $[a] = a^a - a^b$, and the superscripts a and b refer to conditions after and before the shock.

3. Problem formulation II – interaction problem

3.1. *Inspection analysis*

Guided by other triple-deck problems, the estimates of the order of magnitude for the relevant flow quantities are formulated. In particular, it is assumed that the pressure disturbances acting in the interacting boundary layer, i.e. the lower and main decks

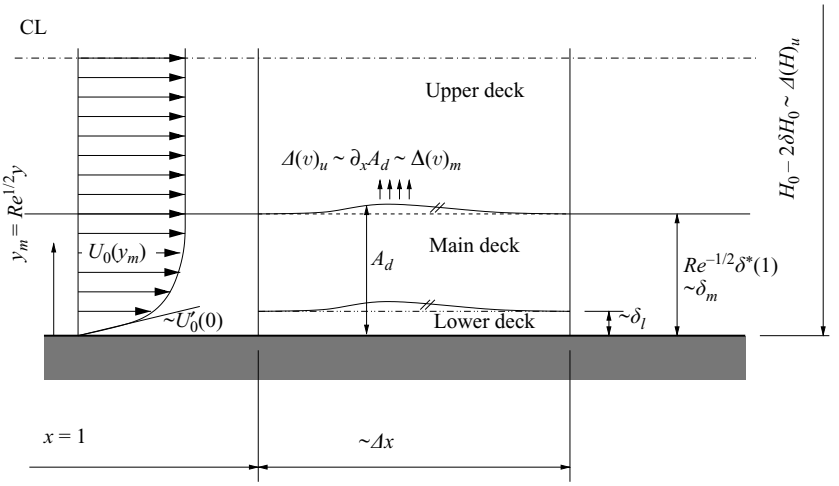

FIGURE 4. Triple-deck structure of interaction region; 'CL' denotes the centreline.

(cf. figure 4), are primarily enforced by the induced pressure disturbances in the upper deck. As is depicted in figure 4 the former core region is represented by a single upper deck which is bounded by the interacting boundary layers from below and above. In the following $(a)_b$ indicates that the flow quantity a is evaluated in the deck denoted by the subscript b, with b being l, m or u for the lower, main or upper deck, respectively, and $0 < \Delta a \ll 1$ denotes a small perturbation of a.

In short, for the lower deck the following assumptions are made: match of the thin-lower-deck with the oncoming boundary layer represented by $U_0(y_m)$ (cf. figure 4), yielding $(u)_l \sim \Delta(u)_l \sim \epsilon \sim U_0'(0)Re^{1/2}\delta_l$, hereby introducing the perturbation parameter $0 < \epsilon \ll 1$ as a measure of the streamwise velocity perturbation in the lower deck; balance of inertia and pressure terms in the x-momentum equation, $\Delta(u)_l^2 \sim \Delta(p)_u \sim \epsilon^2$; balance of inertia and viscous terms in the x-momentum equation, $\Delta(u)_l/\Delta x \sim Re^{-1}\delta_l^{-2}$; and we require a non-degenerate continuity equation, $\Delta(u)_l/\Delta x \sim \Delta(v)_l/\delta_l$. For the passive main deck the assumptions are as follows: balance with lower-deck shift of the velocity profile, $\Delta(u)_m \sim \Delta(u)_l$; exerted displacement on the upper deck, $\Delta(v)_m \sim \Delta(v)_u$; and non-degenerate continuity equation, $\Delta(u)_m/\Delta x \sim \Delta(v)_m/Re^{-1/2}$. The relevant steps of the analysis to establish the dependence of ϵ on the Reynolds number Re have been summarized in table 2 to improve the readability of the text.

In order to obtain the appropriate estimates of the order of magnitude for the upper deck the underlying ideas shall be briefly outlined. The one-dimensional core-region flow is weakly disturbed by the interaction process. The resulting upper-deck flow, in general, is two-dimensional; however, here we seek a distinguished situation in which the channel is sufficiently narrow so that the flow in the upper deck becomes one-dimensional to the leading order. Since the streamwise extent of the interaction region Δx is dependent on the Reynolds number Re, the same has to be true for the channel height $H_0 - 2\delta H_0 \sim \Delta(H)_u$. The key to viscous–inviscid interactions is that the interacting boundary layer affects the inviscid flow in the upper deck and vice versa. In the situation to be considered in the current paper, the single upper deck is confined between the two boundary layers at the channel walls. Consequently the displacement that the interacting boundary layers exert on the upper-deck flow leads to a reduction of the effective flow cross-section for the inviscid core-region flow. Formally one writes $(H)_u(x,t) = H_0 - 2\delta H_0 - 2A_d(x,t) \sim \Delta(H)_u$ for the effective

Inspection analysis	Description
Lower deck:	
$(u)_l \sim \Delta(u)_l \sim \epsilon$	Thin lower deck and no slip at the wall.
$(u)_l \sim U_0'(0) Re^{1/2} \delta_l$	Matching against oncoming boundary layer.
$\Delta(u)_l^2 \sim \Delta(p)_u \sim \epsilon^2$	Balance of inertia and pressure terms in x-momentum equation.
$\Delta(u)_l/\Delta x \sim Re^{-1}\delta_l^{-2}$	Balance of inertia and viscous terms in x-momentum equation.
$\Delta(u)_l/\Delta x \sim \Delta(v)_l/\delta_l$	Non-degenerate continuity equation.
Main deck:	
$\Delta(u)_m \sim \Delta(u)_l$	Balance with lower-deck shift of the velocity profile.
$\Delta(v)_m \sim \Delta(v)_u$	Exerted displacement on the upper deck.
$\Delta(u)_m/\Delta x \sim \Delta(v)_m/Re^{-1/2}$	Non-degenerate continuity equation.
Upper deck:	
$H_0 - 2\delta H_0 \sim \Delta(H)_u$	Channel height depends on one-dimensional limit.
$(H)_u(x,t) = H_0 - 2\delta H_0$ $-2A_d(x,t) \sim \Delta(H)_u$	Boundary-layer displacement A_d reduces flow cross-section $(H)_u(x,t)$.
$\partial_x(H)_u = -2\partial_x A_d \sim \Delta(v)_u$	Boundary-layer displacement induces vertical flow at the leading order (strong interaction).
$\Delta(\rho)_u \sim \Delta(u)_u \sim \Delta(p)_u \sim \epsilon^2$	Degenerate compatibility relation for the right running characteristics.
$\Gamma_0 \sim \epsilon^{2(n-2)}$, $\Lambda_0 \sim \epsilon^{max\{2(n-3),0\}}$, $N_0 \sim 1$	Thermodynamic characterization of a dense gas via the parameter $n \in \{2,3,4\}$ in the relevant flow regime.
$1 - M_0^2 \sim \epsilon^{2(n-1)}$	Transonic flow.
$\epsilon^{2n}/\Delta x \sim \Delta(v)_u/\Delta(H)_u$ and $1/\Delta t \sim \epsilon^{2(n-1)}/\Delta x$	Non-degenerate compatibility relation for the left running characteristics.
$\epsilon^3/\Delta(H)_u \sim \Delta(v)_u/\Delta x$	Irrotational flow.

TABLE 2. Summary of the inspection analysis.

upper-deck channel height, where A_d shall denote the local displacement (cf. figure 4). The reduction of the effective flow cross-section, however, induces a small vertical velocity component in the upper-deck flow, i.e. $\partial_x(H)_u = -2\partial_x A_d \sim \Delta(v)_u$. Now taking a look at the two compatibility relations for one-dimensional compressible isentropic flow (2.8) on the right and left running characteristics $\mathrm{d}x/\mathrm{d}t = u \pm \bar{c}$ and keeping in mind that the core-region flow is transonic, $|u - \bar{c}| \ll u + \bar{c} \sim 1$, we find that the long-term behaviour of the system is characterized by the left running characteristics only. Disturbances moving along the right running characteristics will eventually leave the interaction region in fact 'immediately' when a time scaling of the governing equations preserving the slow-time scales is applied. As a result there is not sufficient time for the right-hand side of the compatibility relation along the right running characteristics accounting for the channel geometry to affect the variation of the field quantities at the leading order. Consequently, as known from other studies of quasi-one-dimensional channel flow, e.g. Chandrasekar & Prasad (1991) and Kluwick & Scheichl (1996), the perturbations of the density, the streamwise velocity and the pressure satisfy $\Delta(\rho)_u \sim \Delta(u)_u \sim \Delta(p)_u \sim \epsilon^2$.

For the purpose of gaining further insight into the long-term flow behaviour we have to consider the compatibility relation for the left running characteristic $\mathrm{d}x/\mathrm{d}t = u - \bar{c}$, i.e.

$$\rho\left(\frac{\partial u}{\partial t} + (u-\bar{c})\partial_x u\right) - \bar{c}\left(\frac{\partial \rho}{\partial t} + (u-\bar{c})\partial_x \rho\right) = \frac{\rho\bar{c}u\partial_x H}{H} + \frac{\rho\bar{c}}{H}\frac{\partial H}{\partial t}, \qquad (3.1)$$

in more detail. The factor $u-\bar{c}=\bar{c}(M-1)$ entering (3.1) can be Taylor expanded about the reference state, i.e. $M=M_0$, $\rho=1$, $c=1$. As shown in Thompson (1971), Cramer (1991) or Kluwick (1993) the variation of M with ρ under isentropic flow conditions is given by

$$\left(\frac{\partial M}{\partial \rho}\right)_s = \frac{M}{\rho}\left(1-\Gamma-\frac{1}{M^2}\right), \tag{3.2}$$

and assuming that the fundamental derivative is expressed in terms of ρ and s, i.e. $\Gamma=\Gamma(\rho,s)$, one finally obtains the expression

$$\bar{c}(M-1) = M_0 - 1 - \Gamma_0(\rho-1) + \frac{1}{2}(\Gamma_0^2-\Gamma_0-\Lambda_0)(\rho-1)^2 + \frac{1}{6}(3\Gamma_0^3-3\Gamma_0^2+14\Gamma_0-4\Lambda_0+5\Gamma_0\Lambda_0-N_0)(\rho-1)^3+\ldots \tag{3.3}$$

for the Taylor expansion of $u-\bar{c}$ about the reference state, introducing the quantities

$$\Lambda = (\partial\Gamma/\partial\rho)_s, \tag{3.4}$$

$$N = (\partial^2\Gamma/\partial\rho^2)_s. \tag{3.5}$$

Let $\Delta(\rho)_u\sim\epsilon^2$ be a measure of the small density disturbances $\rho-1$ which are induced in the interacting core-region flow, i.e. the upper deck. As far as the reference state is concerned three different regimes have to be distinguished in the p versus $1/\rho$-diagram (cf. figure 1b). For states characterized by points in regions $n=2$ in figure 1(b), $\Gamma_0\sim1$, $\Lambda_0\sim1$ and $N_0\sim1$, and the density disturbances are too small to lead to a change in the sign of the fundamental derivative. Consequently, the second and the third term in expression (3.3) represent higher-order corrections and $M_0-1\sim\epsilon^2$. This situation will hereafter be denoted as the case of positive (negative) nonlinearity if $\Gamma>0$ ($\Gamma<0$), since it is the case of a strictly convex (concave) flux function in (3.3). Conversely, a case of mixed nonlinearity denotes a situation in which Γ changes its sign in the flow region of interest, resulting in a non-convex flux function. Note that in the following, we will always use non-convex to indicate the mixed nonlinear behaviour of a function and never in the sense of concave being the opposite of convex, as well. The reference state has to be sufficiently close to the transition line $\Gamma=0$. This is the region denoted by $n=3$ in figure 1(b), where $\Gamma_0\sim\epsilon^2$, $\Lambda_0\sim1$, $N_0\sim1$ and $M_0-1\sim\epsilon^4$, and the region denoted by $n=4$ (close vicinity of the point at which an isentrope touches the transition line in figure 1b) where $\Gamma_0\sim\epsilon^4$, $\Lambda_0\sim\epsilon^2$, $N_0\sim1$ and $M_0-1\sim\epsilon^6$. The argument of a non-degenerate compatibility relation along the left running characteristics (3.1) suggests the balance of the terms $\rho(u-\bar{c})\partial_x u$, $-\rho\bar{c}u\partial_x A_d/H$ and $\rho\partial u/\partial t$ motivating the estimates $\epsilon^{2n}/\Delta x\sim\Delta(v)_u/\Delta(H)_u$ and $1/\Delta t\sim\epsilon^{2(n-1)}/\Delta x$. The last argument concerning the order of magnitude of the upper-deck flow quantities concerns the deviation of the streamlines from the undisturbed oncoming parallel flow expressed by $\Delta(v)_u/\Delta(u)_u$. To this end one writes down the formal asymptotic expansion for $(u)_u\sim1+\epsilon^2u_u^{(1)}+\epsilon^3u_u^{(2)}+\ldots$ and makes the estimate $(v)_u\sim\Delta(v)_u v_u^{(1)}$. Since the $u_u^{(1)}$-field shall be one-dimensional, i.e. depending only on x, the condition of irrotational flow in the upper deck yields the estimate $\epsilon^3/\Delta(H)_u\sim\Delta(v)_u/\Delta x$.

With the given relations for the order of magnitudes of the induced flow quantities in the interaction region (cf. table 2), the small-perturbation parameter ϵ is found to be

$$\epsilon = Re^{-1/(7+2n)}. \tag{3.6}$$

Additionally, one finally obtains the estimates

$$\Delta x \sim \epsilon^3, \quad \delta_l \sim \epsilon^{n+9/2}, \quad \delta_m \sim Re^{-1/2} = \epsilon^{n+7/2}, \quad \Delta(H)_u \sim \epsilon^{-n+9/2} \tag{3.7}$$

for the spatial extent of the various decks and the estimate

$$\Delta t \sim \epsilon^{5-2n} \tag{3.8}$$

for the appropriate time scaling.

The inflow conditions have to be varied such that $\delta H_0 \sim \delta_l \ll Re^{-1/2}$ and $\delta p_0 \sim \Delta(p)_u$.

3.2. *Formal asymptotic expansions and fundamental problem*

For the main deck which comprises most of the interacting boundary layer the inspection analysis suggests

$$x = 1 + \epsilon^3 x_1, \quad y = \epsilon^{n+7/2} y_m, \quad t = \epsilon^{5-2n} t_1, \tag{3.9}$$

where the subscript 1 denotes the quantities used in all three decks, and for the various flow quantities

$$\left.\begin{aligned} (u, v)_m &= (U_0(y_m) + \epsilon u_m^{(1)}(x_1, y_m, t_1) + \ldots,\ \epsilon^{n+3/2} v_m^{(1)}(x_1, y_m, t_1) + \ldots), \\ (\rho)_m &= R_0(y_m) + \epsilon \rho_m^{(1)}(x_1, y_m, t_1) + \ldots, \\ (p)_m &= p_0 + \epsilon^2 p_1^{(1)}(x_1, y_m, t_1) + \ldots. \end{aligned}\right\} \tag{3.10}$$

Here $U_0(y_m)$ and $R_0(y_m)$ represent the velocity and density profiles in the undisturbed boundary layer at $x = 1$. Substitution of (3.10) and (3.9) into the full Navier–Stokes equations (2.1*a*)–(2.1*c*) and taking the limit $Re \to \infty$, one finally finds the classical result that the leading-order perturbations of the velocity components and density are unaffected by the pressure and viscous forces and can be expressed in terms of a (yet-unknown) displacement function $-A_1(x_1, t_1)$

$$u_m^{(1)} = A_1 U_0', \quad v_m^{(1)} = -\partial_{x_1} A_1 U_0, \quad \rho_m^{(1)} = A_1 R_0. \tag{3.11}$$

The crucial points here are that the Grüneisen coefficient G_0 which enters the formulation of the energy equation (2.1*c*) has been found to be $O(1)$ or even $O(\delta)$ for BZT fluids (cf. § 2.1) and that the main-deck problem does not depend explicitly on the time to the leading order under the applied time scaling (3.9). The pressure disturbances

$$p_1^{(1)} = p_1^{(1)}(x_1, t_1) \tag{3.12}$$

are enforced by the induced pressure disturbances in the upper deck and, therefore, do not depend on the lateral distance y_m. The main deck behaves passively and primarily acts to transfer the pressure disturbances generated in the upper-deck flow unchanged to the lower deck and the displacement effects exerted by the lower-deck reaction to the pressure disturbances unchanged back to the upper deck. The displacement effect evoked by the interacting boundary layer which can be seen e.g. by evaluating (3.11) at the edge of the boundary layer,

$$u_m^{(1)} = \rho_m^{(1)} = 0, \quad v_m^{(1)} = -\partial_{x_1} A_1, \quad y_m \to \infty, \tag{3.13}$$

highlighting the notion displacement function for $-A_1$ ultimately leads to a reduction $A_d = Re^{-1/2}\delta^*(1) - \epsilon^{n+9/2} A_1(x_1, t_1)$ of the effective crossflow section for the upper-deck flow,

$$(H)_u = \epsilon^{-n+9/2} H_{01} - 2\left(\epsilon^{n+7/2}\delta^*(1) + \epsilon^{n+9/2}(\delta H_{01} - A_1(x_1, t_1)) + \ldots\right), \tag{3.14}$$

as has been argued in the inspection analysis (cf. figure 4). Here, the term $\epsilon^{n+7/2}\delta^*(1) = Re^{-1/2}\delta^*(1)$ (cf. (3.6)) corresponds to the core-region flow displacement by the oncoming non-interacting boundary-layer flow at $x = 1$ according to classical boundary-layer theory.

For the other relevant flow quantities of the one-dimensional inviscid upper-deck flow we write

$$(u)_u = 1 + \epsilon^2 u_u^{(1)}(x_1, t_1) + \dots, \tag{3.15}$$

$$(\rho)_u = 1 + \epsilon^2 \rho_u^{(1)}(x_1, t_1) + \dots, \tag{3.16}$$

$$(c)_u = 1 + \epsilon^2 c_u^{(1)}(x_1, t_1) + \dots, \tag{3.17}$$

$$(p)_u = p_0 + \epsilon^2 p_1^{(1)}(x_1, t_1) \tag{3.18}$$

and

$$1 - M_0^2 = \epsilon^{2(n-1)} K, \tag{3.19}$$

$$\Gamma_0 = \epsilon^{2(n-2)}\bar{\Gamma}, \quad \Lambda_0 = \epsilon^{max\{2(n-3),0\}}\bar{\Lambda}, \quad N_0 = \bar{N}. \tag{3.20}$$

Here $K = O(1)$ denotes a scaled transonic similarity parameter; for $K > 0$ the oncoming undisturbed core-region flow is subsonic, and for $K < 0$ it is supersonic. Furthermore, $(\bar{\Gamma}, \bar{\Lambda}, \bar{N}) = O(1)$. After insertion of (3.14) and (3.15) into (2.7*a*) and (2.7*b*) one finds

$$u_u^{(1)} = -\rho_u^{(1)} = -p_1^{(1)} \tag{3.21}$$

after integration with respect to x_1 and provided $\delta u_0 = -\delta\rho_0 = -\delta p_0$. The compatibility condition along the left running characteristics (2.8) yields a relationship between the induced pressure disturbances inside the upper deck and the displacement function,

$$\frac{\partial p_1^{(1)}}{\partial t_1} + \frac{1}{2}\frac{\partial}{\partial x_1} J_{[n]}\left(p_1^{(1)}; K, \bar{\Gamma}, \bar{\Lambda}, \bar{N}\right) = -\frac{1}{H_{01}}\frac{\partial A_1}{\partial x_1}, \tag{3.22}$$

making use of expression (3.3) and introducing the perturbation of the mass flux density,

$$J_{[n]}(p; K, \bar{\Gamma}, \bar{\Lambda}, \bar{N}) := \begin{cases} -Kp - \bar{\Gamma}p^2, & n = 2, \\ -Kp - \bar{\Gamma}p^2 - \dfrac{1}{3}\bar{\Lambda}p^3, & n = 3, \\ -Kp - \bar{\Gamma}p^2 - \dfrac{1}{3}\bar{\Lambda}p^3 - \dfrac{1}{12}\bar{N}p^4, & n = 4. \end{cases} \tag{3.23}$$

The displacement function $-A_1(x_1, t_1)$ is an outcome of the solution to the lower-deck problem which is obtained by introducing the following expansions (given here in a form which will eliminate most of the parameters characterizing the unperturbed flow in the resulting distinguished limit):

$$\left.\begin{aligned} (u)_l &= \epsilon R_0(0)^{-1/2}|2\bar{\Gamma}/K|^{-1/2}U(X, Y, T) + \dots, \\ (v)_l &= \epsilon^{n+5/2}\mu_w R_0(0)^{-1/2}U_0'(0)|2\bar{\Gamma}/K|^{1/2}V(X, Y, T) + \dots, \\ (\rho)_l &= R_0(0) + \dots, \\ (p)_l &= p_0 + \epsilon^2|2\bar{\Gamma}/K|^{-1}P(X, T) + \dots, \end{aligned}\right\} \tag{3.24}$$

where

$$(y)_l = \epsilon^{n+9/2}R_0(0)^{-1/2}U_0'(0)^{-1}|2\bar{\Gamma}/K|^{-1/2}(Y + S_{-\infty}) \tag{3.25}$$

and

$$x_1 = \mu_w^{-1} R_0(0)^{-1/2} U_0'(0)^{-2} |2\bar{\Gamma}/K|^{-3/2} X, \tag{3.26}$$

$$t_1 = \mu_w^{-1} R_0(0)^{-1/2} U_0'(0)^{-2} |\Gamma|^{-1} |2\bar{\Gamma}/K|^{-1/2} T, \tag{3.27}$$

$$A_1 = R_0(0)^{-1/2} U_0'(0)^{-1} |2\bar{\Gamma}/K|^{-1/2} (A(X,T) - S_{-\infty}). \tag{3.28}$$

Here $S_{-\infty}$ denotes the scaled variation of the channel height,

$$\delta H_0 = \epsilon^{n+9/2} R_0(0)^{-1/2} U_0'(0)^{-1} |2\bar{\Gamma}/K|^{-1/2} S_{-\infty}, \tag{3.29}$$

and μ_w is the dynamic viscosity evaluated at the channel wall. Insertion into the full Navier–Stokes equation yields the fundamental lower-deck equations in canonical, i.e. parameter-free, form,

$$\frac{\partial U}{\partial X} + \frac{\partial V}{\partial Y} = 0, \quad U\frac{\partial U}{\partial X} + V\frac{\partial U}{\partial Y} = -\frac{\partial P}{\partial X} + \frac{\partial^2 U}{\partial Y^2}. \tag{3.30}$$

These are supplemented by the no-slip condition at the wall,

$$U = V = 0, \qquad Y = 0, \tag{3.31}$$

the conditions of matching with the undisturbed non-interacting boundary layer upstream,

$$U = Y, \quad V = 0, \quad P = P_{-\infty}, \qquad X \to -\infty, \tag{3.32}$$

where $P_{-\infty}$ is the scaled variation of the inflow pressure,

$$\delta P_0 = \epsilon^2 |2\bar{\Gamma}/K| P_{-\infty}, \tag{3.33}$$

and the conditions of matching with the main deck flow,

$$U = Y + A(X,T), \qquad Y \to \infty. \tag{3.34}$$

The quasi-steady lower-deck problem (3.30)–(3.34) is closed by the interaction relation (3.22) which reads in canonical form as

$$-\frac{\partial P}{\partial T} + \frac{\partial}{\partial X} G_{[n]}(P; K, \Gamma_{-\infty}, \Lambda_{-\infty}, N_{-\infty}) = Q\frac{\partial}{\partial X}(A - S_{-\infty}), \tag{3.35}$$

where $G_{[n]}$ is a scaled version of $-J_{[n]}$ defined by

$$G_{[n]}(P; K, \Gamma, \Lambda, N) := \begin{cases} \operatorname{sign}(K)P + \frac{1}{2}\Gamma P^2, & n = 2, \\ \operatorname{sign}(K)P + \frac{1}{2}\Gamma P^2 + \frac{1}{6}\Lambda P^3, & n = 3, \\ \operatorname{sign}(K)P + \frac{1}{2}\Gamma P^2 + \frac{1}{6}\Lambda P^3 + \frac{1}{24} N P^4, & n = 4. \end{cases} \tag{3.36}$$

The parameters entering the canonical formulation, i.e.

$$\Gamma_{-\infty} = \bar{\Gamma}|\bar{\Gamma}|^{-1}, \tag{3.37}$$

$$\Lambda_{-\infty} = \bar{\Lambda}|2\bar{\Gamma}/K|^{-1}|\bar{\Gamma}|^{-1}, \tag{3.38}$$

$$N_{-\infty} = \bar{N}|2\bar{\Gamma}/K|^{-2}|\bar{\Gamma}|^{-1}, \tag{3.39}$$

$$Q = 2^{-1} R_0(0)^{-1/2} U_0'(0)^{-1} |2\bar{\Gamma}/K|^{3/2} |\bar{\Gamma}|^{-1} H_{01}^{-1} > 0, \tag{3.40}$$

are essential parameters to the problem and are therefore not eliminated by the transformation (3.24)–(3.26). Integration of the interaction law (3.35) for steady flows (which are the main focus of the present paper) with respect to X gives

$$G_{[n]}(P) - Q\,(A - S_{-\infty}) = j_1^{(1)} = 0, \tag{3.41}$$

where the dependence of $G_{[n]}$ on the parameters has been suppressed. Evaluation of (3.41) for $X \to -\infty$ taking note of (3.32) and (3.34) indicates that the integration constant $j_1^{(1)}$, in general, depends on the chosen variation of the channel height $S_{-\infty}$ and the inflow conditions $P_{-\infty}$, i.e. $j_1^{(1)} = G_{[n]}(P_{-\infty}) + QS_{-\infty}$. In the following we impose that $j_1^{(1)} = 0$, and consequently the variations $P_{-\infty}$ and $S_{-\infty}$ have to satisfy the compatibility condition,

$$G_{[n]}(P_{-\infty}) + QS_{-\infty} = 0. \tag{3.42}$$

Motivated by physical considerations presented in § 3.3 we henceforth vary the channel height and the inflow conditions in such a way that the mass flux in the oncoming inviscid channel core remains unchanged to the initial situation of a nozzle characterized by the chosen reference states.

3.3. *The interaction relation – links to inviscid theory*

The function $J_{[n]}$ in (3.23) has been introduced as the perturbation mass flux density in the interaction relation (3.22). If A_1 would be a given geometric variation of the channel cross-section instead of the displacement evoked by the interacting boundary layers the interaction relation (3.22) would take on the form of the unsteady transonic small-disturbance equation which describes the long-term propagation of disturbances in inviscid dense-gas flow through a slowly varying channel (cf. Kluwick & Scheichl 1996). The version for steady flows,

$$J_{[n]}\big(p_1^{(1)}; K, \bar{\Gamma}, \bar{\Lambda}, \bar{N}\big) + \frac{A_1}{H_{01}} = \text{constant}, \tag{3.43}$$

would then express the continuity of the perturbation mass flux (cf. Kluwick 1993). Since $G_{[n]}$ is a scaled version of $-J_{[n]}$ the interaction law (3.41) has the same interpretation, and the integration constant $j_1^{(1)}$ in (3.41) has the meaning of a (scaled) perturbation mass flux.

Because of (3.3) the Mach number variation in the interacting channel core during isentropic expansion or compression can be written in the form

$$(M-1)/\epsilon^{2(n-1)} = \frac{1}{2}\mathrm{d}J_{[n]}/\mathrm{d}p_1^{(1)} + \cdots = -4^{-1}|K|^2|\bar{\Gamma}|^{-1}\mathrm{d}G_{[n]}/\mathrm{d}P + \ldots. \tag{3.44}$$

From (3.44) it is evident that the Mach number varies in a non-monotonous manner in case of dense gases exhibiting mixed nonlinearity, i.e. $n = 3$ and $n = 4$.

A stationary normal shock forming in purely inviscid compressible channel flow has to satisfy the Rankine–Hugoniot jump conditions (2.9). In particular, condition (2.9*a*) ensuring the continuity of the mass flux across a shock discontinuity yields the relation

$$\big[G_{[n]}(P; K, \Gamma_{-\infty}, \Lambda_{-\infty}, N_{-\infty})\big] = 0 \tag{3.45}$$

for all possible candidates of flow conditions after the shock P^a for a given flow condition P^b before the shock. Here and in the following we use $G_{[n]}$ instead of $J_{[n]}$ without loss of generality.

In general, the jump relations (2.9) are not sufficient to rule out inadmissible shocks for general fluids exhibiting mixed nonlinearity in the dense-gas regime because of the non-convexity of the mass flux density relation. To this end these have been generalized in Kluwick (1993) for the stationary inviscid nozzle flow of dense gases described by the transonic small-disturbance equation to the shock admissibility criterion which is summarized here in Theorem 3.1.

THEOREM 3.1 (SHOCK ADMISSIBILITY CRITERION, INVISCID FLOW). *A weak stationary normal shock forming in one-dimensional inviscid flow of dense gases, which is governed by the negative perturbation mass flux density* $G_{[n]}$ (3.36)*, is admissible if and only if the following conditions are met:*

(*a*) *The Rayleigh line connecting the states before and after the shock,*

$$\mathscr{C}_R = \{(P, G) : G = G_{[n]}(P^b; K, \Gamma_{-\infty}, \Lambda_{-\infty}, N_{-\infty}), \quad P \in [P^b, P^a]\}, \tag{3.46}$$

does not intersect the intervening branches of the graph,

$$\mathscr{C}_G = \{(P, G) : G = G_{[n]}(P; K, \Gamma_{-\infty}, \Lambda_{-\infty}, N_{-\infty}), \ P \in [P^b, P^a]\}. \tag{3.47}$$

(*b*) *The flow conditions before and after a shock have to satisfy* $M^b \geqslant 1 \geqslant M^a$.

(*c*) *In case of a double-sonic shock,* $M^a = 1 = M^b$*, the shock has to be an expansion shock.*

Shocks which satisfy the shock admissibility criterion (3.1) have been found to be consistent with internal-shock profiles resulting from thermo-viscous regularization in external flows (cf. Cramer & Crickenberger 1991; Kluwick 1993). In the following the shock admissibility criterion shall be discussed in the light of internal-shock profiles resulting from a regularization by viscous–inviscid interactions in internal flows through narrow channels.

4. Analytical results for non-trivial eigensolutions

4.1. *Eigensolutions, internal-shock profiles and pseudo-shocks*

An interesting property of non-trivial eigensolutions to the steady interaction problem (3.30)–(3.34) and (3.41) is that they correspond to the internal structures of weak normal shocks. These have to connect the undisturbed states in the inviscid flow regime before (upstream) the shock discontinuity,

$$P = P^b = P_{-\infty}, \quad A = 0, \quad U = Y, \quad X \to -\infty,$$

with the undisturbed flow states after (downstream) the shock,

$$P = P^a, \quad A = 0, \quad U = Y, \quad X \to \infty.$$

The values of P^b $(= P_{-\infty})$ and P^a thereby have to satisfy the jump condition (3.45) $[G_{[n]}] = G_{[n]}(P^a) - G_{[n]}(P^b) = 0$. On the other hand, in the Introduction we have argued that the shock–boundary-layer interaction should ultimately lead to the formation of a weak pseudo-normal shock in order to motivate the regularizing mechanism of shock–boundary-layer interaction to be expected in internal narrow-channel flows. However, a pseudo-shock, in general, is not an internal-shock profile, since the pressure jump obtained by a pseudo-shock is smaller than that predicted by the purely inviscid theory (cf. Matsuo *et al.* 1999), but in the weak-shock limit $M_0 \to 1$ considered here, as will be discussed in the following, the notion of weak pseudo-shock, internal-shock profile and non-trivial eigensolution to the interaction problem are equivalent and interchangeable.

4.2. *Asymptotic far upstream behaviour*

The upstream behaviour of the stationary interacting flow for $X \to -\infty$ can be investigated by extending the analysis of Lighthill (1953) and Stewartson & Williams (1969), dealing with freely interacting boundary layers in external supersonic flows to incorporate the algebraic interaction law (3.41) and the new matching conditions upstream (3.32). The ansatz

$$\left.\begin{aligned} U &= Y - a_1 \mathrm{e}^{\kappa X} f_1(Y) + \ldots, \quad V = a_1 \kappa \mathrm{e}^{\kappa X} f_1'(Y)) + \ldots, \\ P &= P_{-\infty} + a_1 \mathrm{e}^{\kappa X} + \ldots \end{aligned}\right\} \tag{4.1}$$

with $\exp(\kappa X) \to 0$ for $X \to -\infty$ leads to the expression

$$f_1'(Y) = \int_0^Y \mathrm{Ai}(\kappa^{1/3} s)\, \mathrm{d}s, \qquad f_1(Y) = \int_0^Y \int_0^z \mathrm{Ai}(\kappa^{1/3} s)\, \mathrm{d}s\, \mathrm{d}z \tag{4.2}$$

for f_1 and the well-known result for the displacement function

$$A(X) = \frac{a_1}{3\mathrm{Ai}'(0)} \kappa^{1/3} \mathrm{e}^{\kappa X}, \qquad \mathrm{Ai}'(0) < 0, \tag{4.3}$$

where Ai denotes the Airy function (Abramowitz & Stegun 1970). Substitution of the expressions for P and A into the algebraic interaction law (3.41) and collecting terms $O(\exp(m\kappa X))$ with $m \in \mathbb{N}^0$ yields to the leading order ($m = 0$)

$$G_{[n]}(P_{-\infty}; K, \Gamma_{-\infty}, \Lambda_{-\infty}, N_{-\infty}) = -QS_{-\infty}, \tag{4.4}$$

which is immediately satisfied because of the compatibility assumptions made for the variation of the inflow conditions (3.42). By considering terms $O(\exp(\kappa X))$ one obtains the expression

$$G'_{[n]}(P_{-\infty}; \ldots) := \frac{\mathrm{d}}{\mathrm{d}P} G_{[n]}(P_{-\infty}; K, \Gamma_{-\infty}, \Lambda_{-\infty}, N_{-\infty}) = \frac{Q}{3\mathrm{Ai}'(0)} \kappa^{1/3}, \tag{4.5}$$

yielding a relation for κ:

$$\kappa = \left(G'_{[n]}(P_{-\infty}; \ldots) \frac{3\mathrm{Ai}'(0)}{Q} \right)^3. \tag{4.6}$$

A non-trivial eigensolution to the fundamental problem has to decay for $X \to -\infty$ because of (3.32). Taking note of the sign of $\mathrm{Ai}'(0) < 0$ (cf. Abramowitz & Stegun 1970) and $Q > 0$ (cf. (3.40)), this implies $G'_{[n]}(P_{-\infty}, \ldots) \leqslant 0$. Consequently, the oncoming channel flow has to be supersonic, i.e. $G'_{[n]}(P_{-\infty}, \ldots) < 0$, or sonic in the limiting case $G'_{[n]}(P_{-\infty}, \ldots) \to 0^-$ (cf. (3.44)). In particular, this result, i.e. $M^b \geqslant 1$, is in accordance with the shock admissibility criterion in Theorem 3.1 for inviscid nozzle flow.

4.2.1. *Linear spatial stability of undisturbed flow states*

The generalization of Lighthill's ansatz used before (4.1) can be extended even further in order to study the linear spatial stability of an arbitrary undisturbed flow state represented by $P_{-\infty}$ and $S_{-\infty}$ which always is a trivial solution of the interaction problem (3.30)–(3.34) and (3.41). To this end we write

$$\left.\begin{aligned} U &= \mathrm{Re}\{\hat{U}\} = Y - \mathrm{Re}\{a_1 \mathrm{e}^{\kappa X - \mathrm{i}\omega T} f_1(Y)\} + \ldots, \\ V &= \mathrm{Re}\{\hat{V}\} = \mathrm{Re}\{a_1 \kappa \mathrm{e}^{\kappa X - \mathrm{i}\omega T} f_1'(Y)\} + \ldots, \\ P &= \mathrm{Re}\{\hat{P}\} = P_{-\infty} + \mathrm{Re}\{a_1 \mathrm{e}^{\kappa X - \mathrm{i}\omega T}\} + \ldots, \end{aligned}\right\} \tag{4.7}$$

with $\omega \in \mathbb{R}$ some given harmonic frequency and $\kappa \in \mathbb{C}$ the corresponding unknown complex wavenumber. Furthermore, $X,\ Y, P_{-\infty} \in \mathbb{R}$, $a_1 \in \mathbb{C}$ and $f_1 : \mathbb{R} \to \mathbb{C}$.

By plugging (4.7) into the equation for the quasi-steady lower-deck flow (3.30)–(3.34) one recovers (4.2) for f_1,

$$f_1'(Y) = \int_0^Y \mathrm{Ai}(\kappa^{1/3}s)\,\mathrm{d}s, \qquad f_1(Y) = \int_0^Y \int_0^z \mathrm{Ai}(\kappa^{1/3}s)\,\mathrm{d}s\,\mathrm{d}z,$$

with the main difference that $\kappa \in \mathbb{C}$ herein. From the asymptotic properties of the Airy function $\mathrm{Ai}(z)$ for $z \in \mathbb{C}$ and $|z| \to \infty$ one infers that the integrals exist for $Y \to \infty$ only if $\kappa \in \{z \in \mathbb{C} : |\mathrm{Arg}(z)| \leqslant \pi/3\}$. Evaluating the matching condition (3.34) then leads to

$$A = \mathrm{Re}\{\hat{A}\} = \mathrm{Re}\left\{\frac{a_1}{3\mathrm{Ai}'(0)}\kappa^{1/3}\mathrm{e}^{\kappa X - \mathrm{i}\omega T}\right\}, \tag{4.8}$$

and after insertion into the linearized interaction law for unsteady flow one finally obtains a relation between the harmonic frequency and the complex wavenumber,

$$\mathrm{i}\omega + G_{[n]}'(P_{-\infty})\kappa = \frac{Q}{3\mathrm{Ai}'(0)}\kappa^{4/3}, \tag{4.9}$$

where the dependence of $G_{[n]}$ on the parameters K, $\Gamma_{-\infty}$, $\Lambda_{-\infty}$, $N_{-\infty}$ has been suppressed. Provided $G_{[n]}'(P_{-\infty}) \neq 0$, (4.9) can be written in the manner

$$\mathrm{i}\bar{\omega} + \bar{\kappa} = \mathrm{sign}(\mathrm{Ai}'(0)G_{[n]}'(P_{-\infty}))\bar{\kappa}^{4/3}, \tag{4.10}$$

introducing a modified definition of the harmonic frequency and of the wavenumbers, $\bar{\omega}$ and $\bar{\kappa}$,

$$\bar{\omega} = C\frac{\omega}{G_{[n]}'(P_{-\infty})} \in \mathbb{R}, \qquad \bar{\kappa} = C\kappa \in \mathbb{C}, \tag{4.11}$$

with

$$C = \left|\frac{Q}{3\mathrm{Ai}'(0)G_{[n]}'(P_{-\infty})}\right|^3 > 0. \tag{4.12}$$

Note that the new definition $\bar{\kappa}$ for the wavenumber is only a rescaling of κ, i.e. $\mathrm{Arg}(\kappa) = \mathrm{Arg}(\bar{\kappa})$. Interestingly enough, for the discussion of (4.10) only two cases have to be considered, i.e. $G_{[n]}' < 0$ and $G_{[n]}' > 0$. That is to say one simply has to distinguish between supersonic and subsonic flows.

A candidate for a solution to (4.10) for a given $\bar{\omega}$ can be obtained by finding the roots of the polynomial

$$\mathrm{sign}(\mathrm{Ai}'(0)G_{[n]}'(P_{-\infty}))\bar{\kappa}^4 - \bar{\kappa}^3 - 3\mathrm{i}\bar{\omega}\bar{\kappa}^2 + 3\bar{\omega}^2\bar{\kappa} + \mathrm{i}\bar{\omega}^3 = 0 \tag{4.13}$$

which are plotted in figure 5. From the four possible wavenumbers $\bar{\kappa}$ for a given harmonic frequency $\bar{\omega}$ only those that lie in the set $\Omega_\kappa = \{z \in \mathbb{C} : |\mathrm{Arg}(z)| \leqslant \pi/3\}$, depicted by the shaded regions in figure 5, lead to a non-trivial solution of the lower-deck problem, as has been noted before. On the other hand, linear spatial stability of the trivial solution requires that the real part of $\bar{\kappa}$ has to be negative, $\mathrm{Re}\{\bar{\kappa}\} < 0$; i.e. some disturbance generated at a purely harmonic frequency $\bar{\omega}$ is dying out downstream. In case of $\mathrm{Re}\{\bar{\kappa}\} > 0$ the disturbances are growing exponentially downstream until nonlinearity takes over.

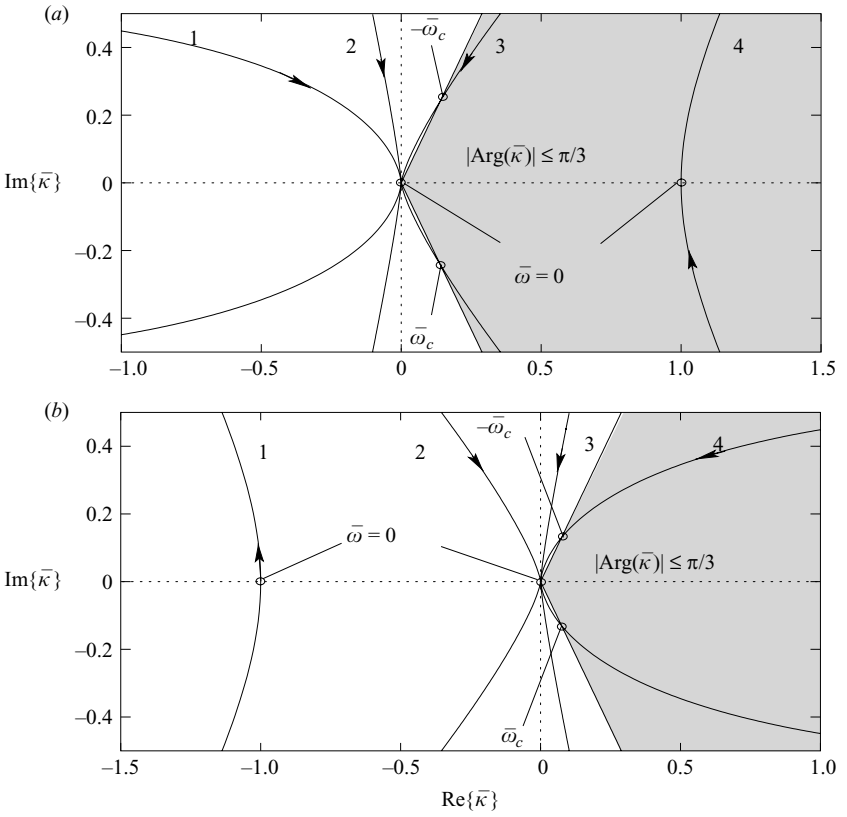

FIGURE 5. Roots $\bar{\kappa}$ of (4.10) under variation of $\bar{\omega}$ for (*a*) supersonic, i.e. $G'_{[n]}(P_{-\infty}) < 0$, and (*b*) subsonic, i.e. $G'_{[n]}(P_{-\infty}) > 0$, undisturbed initial flow.

Keeping that in mind, figure 5 can be interpreted in the following way. Taking a look at figure 5(*a*), the case of a supersonic trivial solution of the interaction problem, and setting $\bar{\omega} = 0$, i.e. applying a steady disturbance, one obtains the result $\bar{\kappa}_{1,2,3} = 0$ for the first three wavenumbers, which is the trivial solution again, and $\bar{\kappa}_4 = 1 \in \mathbb{R}$; $\bar{\kappa}_4$ lies within the set Ω_κ, and therefore ansatz (4.7) leads to a non-trivial solution for $\bar{\kappa}_4$ which results in disturbances growing downstream because of $\mathrm{Re}\{\bar{\kappa}\} > 0$. Making use of (4.11), result (4.6) based on Lighthill's ansatz (4.1) is retrieved. For $\bar{\omega} \in [-\bar{\omega}_c, \bar{\omega}_c]$ there exists only the one non-trivial solution on branch 4 which is exponentially growing downstream. For $|\bar{\omega}| > \bar{\omega}_c$ the second branch, branch 3 in figure 5(*a*), enters the region Ω_κ.

The situation in the case of a subsonic trivial solution of the interaction problem is quite different (see figure 5*b*). For $\bar{\omega} = 0$ no non-trivial growing mode can exist since $\bar{\kappa}_{1,2,3,4} \notin \Omega_\kappa$. This situation does not change as long as $\bar{\omega} \in [-\bar{\omega}_c, \bar{\omega}_c]$. However, as soon as $|\bar{\omega}| > \bar{\omega}_c$, branch 4 enters Ω_κ and a growing mode exists besides the trivial flow state.

Therefore we conclude that the supersonic trivial flow state, i.e.

$$P = P_{-\infty}, \quad A = 0, \quad U = Y, \quad G'_{[n]}(P_{-\infty}) < 0,$$

is unconditionally unstable according to the concept of linear spatial stability, and the subsonic trivial flow state, i.e.

$$P = P_{-\infty}, \quad A = 0, \quad U = Y, \quad G'_{[n]}(P_{-\infty}) > 0,$$

is stable as long as the harmonic frequency of the disturbance satisfies the condition $|\bar{\omega}| < \bar{\omega}_c$.

4.3. *Asymptotic far downstream behaviour*

The investigation of the downstream behaviour of the steady interacting flow closely follows the analysis by Kluwick *et al.* (2009) who applied the results derived by Gittler (1992), which described the asymptotic properties of a very general class of steady triple-deck problems in the limiting cases of $Y \gg 1$ and $X \gg 1$ to a triple-deck problem with a local interaction law, closely resembling (3.41) and describing weakly nonlinear bores in laminar high-Reynolds-number flow. The significant and fundamental difference from the interaction problem considered in this treatise is, besides the different underlying physics involved, that their interaction law accounts only for terms of quadratic nonlinearity in the pressure and that, additionally, a dispersive term is present in their relation.

As a starting point the stream function $\Psi(X, Y)$: $U = \partial\Psi/\partial Y$, $V = -\partial\Psi/\partial X$ is expanded for $Y \to \infty$,

$$\Psi(X, Y) \sim \frac{1}{2}(Y + A(X))^2 + P(X) + K_{rs} Y^r (\ln Y)^s + \dots \tag{4.14}$$

with $r < 2$. This expression is valid for all X and contains free constants K_{rs}. Since the flow structure far upstream is given by (4.1) and (4.2), the corresponding velocity disturbances $U - Y$, V decay exponentially with $Y \to \infty$ because of the asymptotic properties of the Airy function (see Abramowitz & Stegun 1970). Consequently the algebraic terms in Y in (4.14) vanish, $K_{rs} = 0$. Therefore, if the assumption that the interacting flow approaches an undisturbed state downstream is correct, then Ψ has to take on the following form far downstream:

$$\Psi(X, Y) \sim \frac{1}{2}Y^2 + A(X)Y + P^a + \dots, \qquad X \to \infty,\ Y \to \infty. \tag{4.15}$$

This result has to be compared with the similarity form of the stream function far downstream (Gittler 1992),

$$\Psi(X, Y) \sim \frac{1}{2}Y^2 + \alpha X^\beta f_2(\eta) + C_2 X^\lambda h_2(\eta) + \cdots, \qquad \eta = \frac{Y}{X^{1/3}}. \tag{4.16}$$

If as in the present case no external agencies are affecting the flow under consideration (no surface-mounted obstacle, say), then the parameter $\alpha = 0$, thereby eliminating the second term in (4.16). The third term represents a homogeneous eigensolution with the eigenvalue λ, and its asymptotic behaviour of $h(\eta)$ for $\eta \to \infty$ has been given in Gittler (1992):

$$h(\eta) \sim K_1\eta + K_2\eta^{3\lambda} + K_3 e^{-3\lambda-4} e^{-\eta^2/9} + \dots, \qquad \eta \to \infty. \tag{4.17}$$

The two constants K_1 and K_3 are arbitrary while

$$K_2 = \frac{\Gamma\left(\frac{2}{3}\right) 3^{-2\lambda+1/3}}{(3\lambda - 1)\Gamma(\lambda + 1)} \tag{4.18}$$

with $\Gamma(\cdot)$ denoting the Gamma function. Therefore, in the end a second expression describing the properties of Ψ in the limit $X \to \infty$, $Y \to \infty$ is obtained:

$$\Psi(X, Y) \sim \frac{1}{2}Y^2 + C_2 K_1 X^{\lambda-1/3} Y + C_2 K_2 Y^{3\lambda} + \dots, \qquad X \to \infty,\ Y \to \infty. \tag{4.19}$$

Comparison of (4.15) and (4.19) for Ψ implies $\lambda = 0$ and

$$A(X) \sim C_2 K_1 X^{-1/3} + \ldots, \qquad X \to \infty. \tag{4.20}$$

Finally, substitution of (4.20) into the linearized interaction law for steady flow (3.41) yields the asymptotic behaviour of the pressure far downstream. Provided $G'_{[n]}(P^a) \neq 0$ it takes on the form

$$P(X) \sim P^a + \frac{QC_2K_1}{G'_{[n]}(P^a)} X^{-1/3} + \ldots, \qquad X \to \infty, \tag{4.21}$$

again suppressing the dependence of $G_{[n]}$ on the scaled parameters K, $\Gamma_{-\infty}$, $\Lambda_{-\infty}$ and $N_{-\infty}$. However, if the shock terminates in a sonic flow state far downstream, i.e. $G'_{[n]}(P^a) = 0$, then the asymptotic behaviour of the pressure is given by

$$P(X) \sim P^a + \operatorname{sign}(G''(P^a)) \left(\frac{2QC_2K_1}{G''_{[n]}(P^a)} \right)^{1/2} X^{-1/6} + \ldots, \qquad X \to \infty, \tag{4.22}$$

indicating an even weaker algebraic decay of the pressure than in (4.21).

Most important of all, a non-trivial eigensolution of the interaction problem approaches an undisturbed flow state downstream of the interaction region at a pressure P^a which is predicted by inviscid theory, i.e. $[G_{[n]}] = 0$. Moreover, the requirement that the Rayleigh line connecting the states before and after an admissible shock does not intersect the intervening branches of the graph $\mathscr{C}_G = \{(P, G_{[n]}(P)) \mid P \in [P^b, P^a]\}$ (cf. Theorem 3.1) can be motivated too. Since a non-trivial eigensolution can only exist for supersonic flow conditions upstream, i.e. $G'_{[n]}(P^b) < 0$ (cf. § 4.2), the first undisturbed state, which a fluid particle passing through the interaction region is approaching far downstream, is bound to be subsonic or sonic, i.e. $G'_{[n]}(P^a) \geqslant 0$ and $M^a \leqslant 1$. On the other hand, the results of § 4.2 show that the subsonic undisturbed flow state is stable according to the concept of linear spatial stability at least for disturbances at a harmonic frequency below some bound $\bar{\omega}_c$. Consequently, without the action of external agencies like a variation of the channel throat area the fluid particle is attracted towards the undisturbed subsonic flow state and will not pass through it, and the Rayleigh line will not cross the graph $\mathscr{C}_G$.

We thus conclude that the admissibility criterion theorem, Theorem 3.1, formulated for the case of inviscid flows is automatically satisfied by the internal profiles of regular and sonic shocks resulting from the regularization because of viscous–inviscid interactions of the type considered here. However, the last issue of Theorem 3.1 stating that a double-sonic shock is bound to be a rarefaction shock can only be clarified by studying numerical results.

5. Numerical results for non-trivial eigensolutions

5.1. *Numerical method*

The fundamental problem (3.30)–(3.34) and (3.41) is integrated using a finite-difference scheme of second order and by applying a marching technique downstream in X-direction, the main flow direction, starting from an initial velocity profile reflecting the asymptotic flow behaviour of non-trivial eigensolutions far upstream (cf. § 4.2).

To this end, a new variable $\bar{U} := U - Y$ is introduced, whereas V in the momentum equation in X-direction is expressed by integration of the continuity equation (3.30),

$$V(X, Y) = -\int_0^Y \frac{\partial \bar{U}}{\partial X}(X, \bar{Y})\,\mathrm{d}\bar{Y}. \tag{5.1}$$

With the mapping of Y on to the computational domain $\eta \in [0, 1]$,

$$Y(\eta) = Y_s \left(\frac{1}{1 - \alpha_s \eta} - \frac{1}{1 + \alpha_s \eta} \right),$$

including the scaling parameters α_s, Y_s, the representation of the numerical grid in the new coordinates (X, η) is introduced:

$$(X_i, \eta_j) = (X_0 + i\Delta X_i, j\Delta\eta), \quad i \in \mathbb{N}^0, \ j = 0, \ldots, N_j,$$

where the step size in X-direction, ΔX_i, is adaptable and the step size in, η-direction $\Delta\eta = 1/N_j$, is fixed. Here, X_0 represents some initial value which is no loss of generality because of the translation invariance of the eigensolutions. Specifically, values $\alpha_s = 0.75$, $Y_s = 20.0$ and $\alpha_s = 0.75$, $Y_s = 10.0$ have been adopted to obtain results for $n = 2,\ 3$ in §§ 5.3, 5.4 and 5.5 and for $n = 4$ in §§ 5.6 and 5.7, respectively. The derivatives in X-direction are resolved by means of a Crank–Nicholson discretization, making use of the known/old velocity profile evaluated upstream at X_{i-1} and the unknown/new velocity profile downstream at the next grid point at X_i. For the derivatives in η-direction central differences evaluated at the grid point η_j are used, and for the numerical evaluation of integral (5.1) the trapezoidal rule is applied. The matching condition (3.34) is implemented as

$$A = \bar{U}(X, Y_{max} = Y(1)).$$

This is justified because of the exponential decay of $\bar{U}$ for $Y \gg 1$, which one infers from the asymptotic representation of the stream function Ψ for $Y \gg 1,\ \forall X$ (see the discussion following (4.14)). The results of the numerical calculations presented in §§ 5.3, 5.4 and 5.5 have been obtained by choosing the values $Y_{max} = 68.57$ and $Y_{max} = 34.29$ in §§ 5.6 and 5.7. The number of grid points in η-direction $N_j = 200$.

In the rare cases in which separation occurs, the FLARE approximation (Reyhner & Flügge 1968) has been applied, which yields reasonable good results as long as the region of separated flow remains small (cf. Anderson, Tannehill & Pletcher 1997).

5.2. *Calculation of material parameters for PP10*

Because of the canonical form of the fundamental problem, its solutions are independent of the specific physical values for the parameters governing the channel geometry and working medium. However, it is instructive to choose a definitive physical set-up for numerical experiments in order to verify that the proposed scalings do indeed lead to sensible numerical values for the scaled material parameters, $\Gamma_{-\infty}$, $\Lambda_{-\infty}$, $N_{-\infty}$ and Q, in case of realistic working media, inflow conditions and geometric dimensions.

As an example medium for a possible candidate of a BZT fluid, PP10 ($C_{13}F_{22}$) has been chosen. Guardone & Argrow (2005) commented on the expected thermal stability of PP10 and presented more recent material properties, summarized in table 3, than can found in the earlier publications (Cramer 1989, 1991). Another promising class of media suitable for experimental usage are siloxanes (cf. Colonna *et al.* 2007).

The fundamental derivative is a secondary thermodynamic quantity; i.e. it cannot be accessed by direct measurements, or in case of numerical calculations, partial

Commercial name	Chemical formula	$\tilde{M}$ (g mol^{-1})	$\tilde{\theta}_c$ (K)	$\tilde{P}_c$ (atm)	Z_c	$\tilde{\theta}_b$ (K)	$\tilde{c}^c_{v,\infty}/\tilde{R}_g$	m	ω
PP10	$C_{13}F_{22}$	574	630.2	16.2	0.2859	467	78.37	0.5255	0.4833

TABLE 3. Experimental data for PP10 (Guardone & Argrow 2005): $\tilde{M}$ is the molecular weight, $\tilde{P}_c$ the critical pressure, $\tilde{\theta}_c$ the critical temperature, Z_c the critical compressibility factor, $\tilde{\theta}_b$ the boiling temperature at 1 atm, $\tilde{c}^c_{v,\infty}$ the specific heat for dilute states ($\rho \to 0$) at $\tilde{\theta}_c$, $\tilde{R}_g$ the specific gas constant, m the exponent in (5.3) and ω the acentric factor.

derivatives of the thermodynamic state variables $\tilde{p}$ and $\tilde{\rho}$ have to be calculated for isentropic flow conditions (cf. the definition of Γ in (1.1)). To this end, a functional representation of the thermodynamical equation of state for PP10 has to be chosen. Here, we use the Martin–Hou equation of state (Martin & Hou 1955), since it is reasonably realistic in predicting regions of negative Γ using a small number of experimental data and is applicable with acceptable numerical efforts. The Martin–Hou equation of state is a thermal equation of state, i.e. an incomplete form of an equation of state in the sense that it provides a function for $\tilde{p} = \tilde{p}(\tilde{\theta}, \tilde{\rho})$ only, and therefore, the thermodynamic characterization of the fluid under consideration has to be completed by providing a caloric equation of state:

$$\tilde{e}(\tilde{\theta}, \tilde{\rho}) = \tilde{e}_r + \int_{\tilde{\theta}_r}^{\tilde{\theta}} \tilde{c}_{v,\infty}(\tau)\,\mathrm{d}\tau + \int_{\tilde{\rho}_r}^{\tilde{\rho}} \left(\tilde{\theta}\frac{\partial \tilde{p}}{\partial \tilde{\theta}}(\tilde{\theta}, \varrho) - \tilde{p}(\tilde{\theta}, \varrho) \right) \mathrm{d}\left(\frac{1}{\varrho}\right), \tag{5.2}$$

(cf. Martin & Hou 1955; Guardone & Argrow 2005). Here $\tilde{e}$ denotes the specific inner energy; the subscript r specifies some reference state; and the subscript ∞ indicates that the quantity is evaluated for dilute states, i.e. $\tilde{\rho} \to 0$. Following Thompson & Lambrakis (1973) the functional form of $\tilde{c}_{v,\infty}(\tilde{\theta})$ in the neighbourhood of the critical temperature is approximated by a power law

$$\tilde{c}_{v,\infty} \simeq \tilde{c}^c_{v,\infty} \left(\frac{\tilde{\theta}}{\tilde{\theta}_r} \right)^m. \tag{5.3}$$

The numerical implementation of the equations of state for the calculation of Γ and its higher derivatives Λ and N then follows the study by Colonna & Silva (2003), which moreover gives a very comprehensive selection of various thermodynamic expressions applicable for the calculation of secondary thermodynamic quantities.

The dynamic viscosity has been calculated using the method of Chung *et al.* (1988) for non-polar fluids. The data used are listed in table 3. The method itself as well as the used data have to be taken with caution (cf. Kluwick 1994) in case of dense gases. However, the main purpose here simply is to provide numeric values of realistic magnitude.

Finally, one has to make assumptions on the position of the interaction region in the channel. For the numerical results presented in the following sections we assume that the interaction region is located at $\tilde{L}_0 = 1$ m from the channel entry.

The properties R_0, μ_w and $U_0'(0)$ of the oncoming undisturbed boundary layer needed in the affine transformation (3.24)–(3.26) and in (3.40) are obtained by considering the compressible boundary-layer equations over a semi-infinite flat plate in the limit of dense gases with relatively large specific heats, $\tilde{R}_g/\tilde{c}_v \to 0$. Kluwick (1994) has shown that in the case of a plane uniform flow past a semi-infinite adiabatic flat plate the temperature field and consequently the density field turn out

	p_0/p_c	ρ_c/ρ_0	θ_0/θ_c	$\tilde{u}_0$ (m s^{-1})	$\tilde{\mu}_0$ (Pa s)	K	Γ_0	Λ_0	N_0	Re
§ 5.3	1.0268	1.240	1.00490	28.1	3.67×10^{-5}	−1	1.00	–	–	3.88×10^{8}
§ 5.4	0.949	1.710	0.997	35.5	3.00×10^{-5}	−1	−0.115	–	–	4.36×10^{8}
§ 5.5	0.914	1.917	0.994	40.2	2.80×10^{-5}	−1	−0.0512	−0.918	–	4.71×10^{8}
§ 5.6	0.942	1.850	1.00023	40.1	2.87×10^{-5}	−1	0.0134	−0.455	6.48	4.75×10^{8}
§ 5.7	0.945	1.84	1.00042	39.8	2.88×10^{-5}	−1	0.0110	−0.407	6.90	4.72×10^{8}

	ϵ	Δx	δ_l	δ_m	$\Delta(H)_u$	$\Gamma_{-\infty}$	$\Lambda_{-\infty}$	$N_{-\infty}$	Q_1
§ 5.3	0.166	0.00455	8.42×10^{-6}	5.08×10^{-5}	0.0112	1.00	–	–	4.26
§ 5.4	0.133	0.0235	2.014×10^{-5}	1.52×10^{-4}	0.0645	−1.00	–	–	24.9
§ 5.5	0.215	0.00997	9.93×10^{-6}	4.61×10^{-5}	0.0999	−1.00	−0.375	–	4.48
§ 5.6	0.264	0.0184	1.21×10^{-5}	4.59×10^{-5}	0.514	−1.00	−0.434	0.0761	7.08
§ 5.7	0.264	0.0184	1.21×10^{-5}	4.59×10^{-5}	0.514	−1.00	−0.563	0.141	6.44

TABLE 4. Selected inflow conditions at the channel entry and the resulting scaled parameters for the interaction problem; $Q_1 = Q(H_{01} = 1)$.

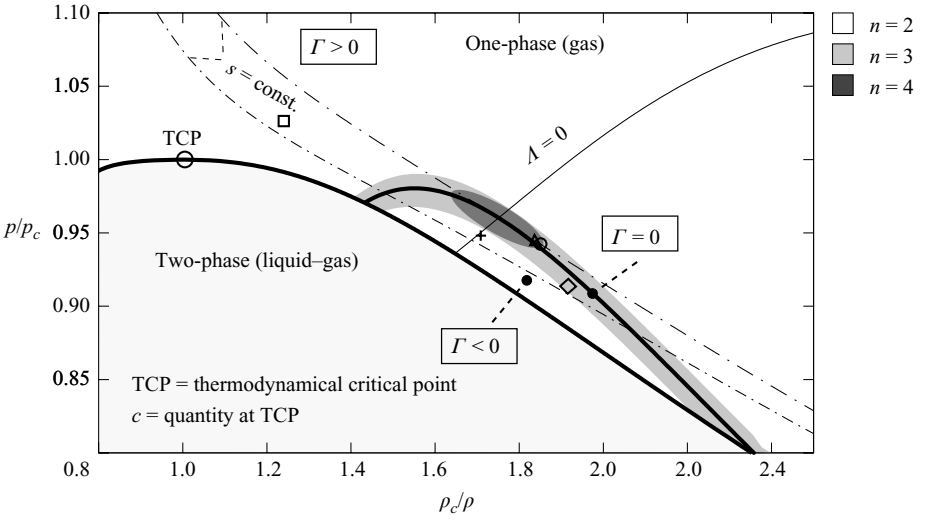

FIGURE 6. Reduced pressure versus reduced-density diagram for PP10 according to the Martin–Hou equation of state. The symbols mark the pressure and density at the channel entry used in the numerical calculations. The symbols are as follows: □, example 1, § 5.3; +, example 2, § 5.4; ◇, example 3, § 5.5; ○, example 4, § 5.6; △, example 5, § 5.7. Furthermore, n indicates the nonlinearity in the pressure to be considered in the interaction law.

to be almost constant in the whole boundary layer, reflecting the fact that for fluids with relatively large specific heats isentropic changes of the thermodynamic state only lead to correspondingly small changes of the temperature (Kluwick 2004). Therefore, $R_0 = 1$ and $\mu_w = 1$, and the boundary-layer flow is described by the well-known Blasius similarity solution with $U_0' = 0.332$ (cf. Kluwick 1994).

The pressure-versus-density diagram in figure 6 shows the various pressure–density pairs at the channel entry, used for the numerical calculations in the following sections, and table 4 summarizes the inflow conditions and the numerical values of the scaled parameters.

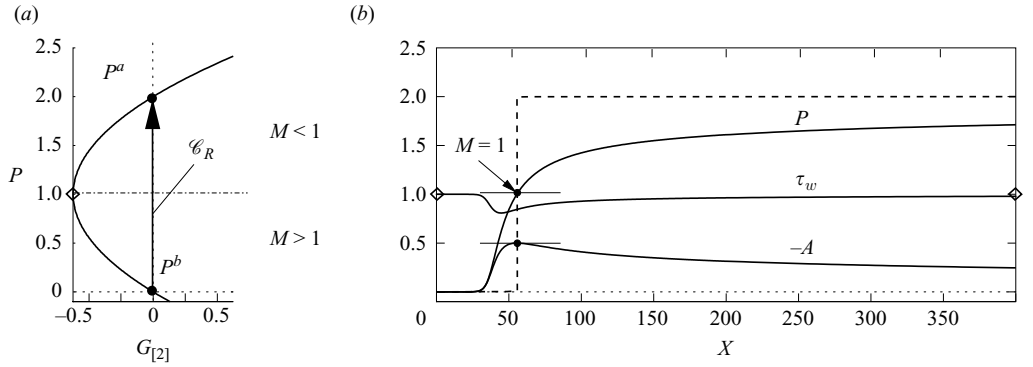

FIGURE 7. (*a*) Plot of the mass flux density $G_{[2]}$ for quadratic nonlinearity in the pressure and Rayleigh line connecting the pressure before and after the shock, P^b and P^a. (*b*) Plot of the perturbation of the pressure, displacement thickness and wall shear τ_w for $Q=1$, $S_{-\infty}=0$.

5.3. *Compression pseudo-shock*

Here we summarize the numerical results for internal profiles of compression shocks (cf. table 4 and figure 6 for the selected inflow conditions and scaled quantities). In figure 7(*a*) the resulting negative mass flux density perturbation $G_{[2]}$ versus the pressure P is shown. As stated in Theorem 3.1, the values of the pressure before and after the shock, P^b and P^a, are connected by the Rayleigh line $\mathscr{C}_R$. The arrow indicates the transition from supersonic flow to subsonic flow as required by the admissibility criterion. Sonic flow conditions indicated by the symbol $\diamond$ are obtained at $P=1$, where $G_{[2]}$ exhibits an extremum. The shock discontinuity in the pressure predicted by purely inviscid theory is sketched in figure 7(*b*), indicated by the dashed lines. The shock discontinuity resolves into a smooth transition from supersonic flow to subsonic flow the moment the interacting boundary layers at the channel walls are considered (cf. the pressure, displacement thickness and wall shear stress distribution τ_w in figure 7). Figure 7 immediately suggests a physical interpretation of the shock regularization mechanism. Assume the distribution of the displacement thickness $-A$ to be a given function of X; then the interaction law (3.41) would describe the inviscid flow of dense gases through a nozzle of variable throat area (cf. § 3.3). However, in contrast with a nozzle of fixed geometry the flow in the boundary layers adjacent to the solid walls and thus $-A$ has the possibility to adapt to the local pressure acting in the interaction region. Since the pressure in a compressive pseudo-shock is increasing monotonously, $\mathrm{d}P/\mathrm{d}X \geqslant 0$, the flow passing through the upper deck is decelerated throughout the interaction region (cf. (3.21)). This is brought about by a reduction of the effective throat area, i.e. by an increase of the disturbance of the displacement thickness, $\mathrm{d}(-A)/\mathrm{d}X > 0$, in the part of the upper deck where the flow is supersonic. A smooth transition of the upper-deck flow through the sonic state characterized by $P=1$ can only be effected if at the same time the effective throat exhibits an extremum, i.e. $\mathrm{d}(-A)/\mathrm{d}X = 0$ (see figure 7). After the sonic state has been transversed the upper-deck flow is subsonic, and a further deceleration is achieved by a successive decrease of $\mathrm{d}(-A)/\mathrm{d}X < 0$. On the other hand, the displacement effect characterized by $-A$ originates from the lower deck reacting to the acting induced pressure gradient. Because of the small velocities close to the walls the flow in the lower deck behaves in an incompressible manner, and consequently, the reduction of the effective throat area for the upper-deck flow,

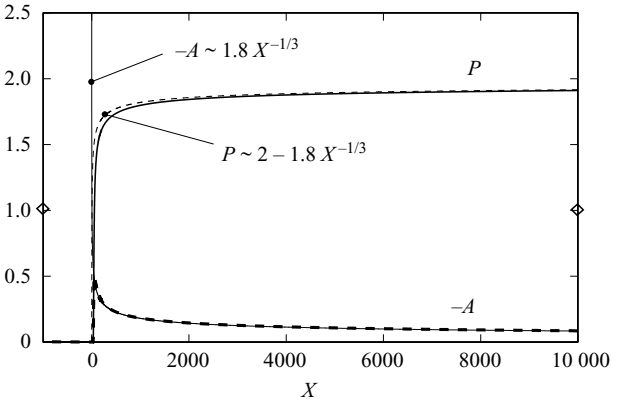

FIGURE 8. Plot of the pressure P and displacement thickness $-A$ for $Q=1$, $S_{-\infty}=0$ and comparison of the asymptotic behaviour far downstream $X \gg 1$ (cf. (4.20) and (4.21)).

corresponding to $\mathrm{d}(-A)/\mathrm{d}X > 0$, is brought about by a deceleration of the lower-deck flow and the increase, i.e. $\mathrm{d}(-A)/\mathrm{d}X < 0$, by an acceleration. To be more specific, from (3.34) we observe $\mathrm{d}U(X, Y \to \infty)/\mathrm{d}X = \mathrm{d}A(X)/\mathrm{d}X$ from which follows the presented interpretation of the lower-deck flow reaction. Finally, the undisturbed flow profile is reached again far downstream. In other words, the viscous boundary layers are forming a 'viscous' Laval nozzle as they adapt to and at the same time interact with the inviscid channel core flow. By reducing or expanding the effective throat area which the upper-deck flow feels, they ensure a smooth transition of the flow from supersonic to subsonic conditions and thereby regularize a possible shock discontinuity in the inviscid upper-deck flow.

In figure 8 the numerical results for an internal-shock profile are compared with the analytical results for the asymptotic far-downstream behaviour obtained in § 4.3. To this end, (4.20) is fitted to the numerical results, delivering the numerical value for C_2K_1. In the next step the coefficient in (4.21) can be calculated. Good agreement is observed.

Figure 9, on the other hand, shows the influence of the parameter Q entering the interaction law on the distribution of the pressure, displacement thickness and wall shear stress. By reducing Q, i.e. by reducing the strength of the regularizing effect of viscous–inviscid interaction, the pressure profile more and more seems to approach the discontinuous solution of a shock, again depicted by the dashed lines. However, this forces an increasingly stronger reaction of the lower-deck flow as is revealed by inspecting the plot of the displacement thickness in figure 9. Because of the unfavourable effect of an adverse pressure gradient acting in a compressive shock profile on the boundary-layer flow the minimum of the wall shear stress decreases with the increasing steepness of the pressure profile. This finally causes the formation of local separated flow regions as evidenced by the results for the smallest value of $Q=0.2$ included in figure 9.

5.4. *Rarefaction pseudo-shock*

As a second numerical example the internal profile of a rarefaction shock which is expected to exist in case of $\Gamma < 0$ is considered in this section (cf. table 4 and figure 6 for the selected inflow conditions).

In figure 10(a) the negative perturbation of the mass flux density $G_{[2]}$ versus the pressure P is shown, which is strictly concave in the case of negative nonlinearity.

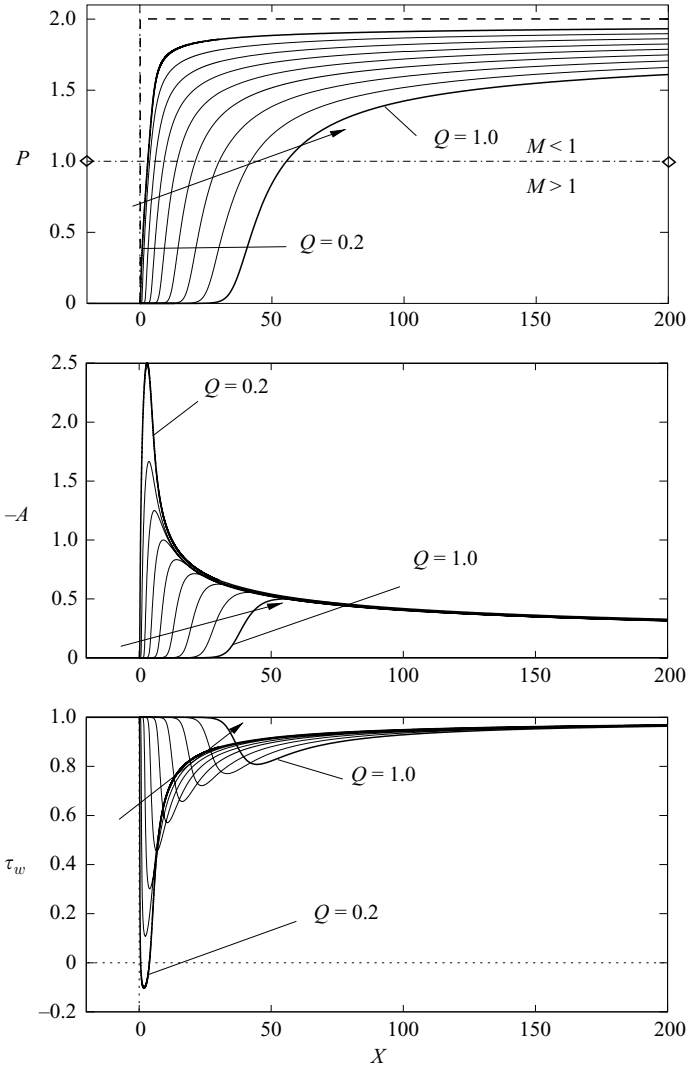

FIGURE 9. Distributions of the pressure, displacement thickness and wall shear stress in an internal-shock profile connecting P^b and P^a for various values of Q and $S_{-\infty}=0$; $Q=0.2, 0.3, \ldots, 1.0$.

Application of the shock admissibility criteria in Theorem 3.1 indicates that a rarefaction shock is the admissible type of shock for this flow configuration, as it leads to a transition from supersonic to subsonic flow conditions. (It is noteworthy that even though the core-region flow is accelerated because of $\mathrm{d}P/\mathrm{d}X<0$ a net decrease of the local Mach number is achieved, as the increase of the flow velocity is overcompensated by the increase of the local speed of sound if $\Gamma<1$; cf. Thompson 1971.) As before, the pressure discontinuity occurring in the case of inviscid flows is indicated by the dashed lines. Again, the shock discontinuity resolves into a smooth internal-shock profile if the interacting boundary layers at the walls are taken into account.

The influence of the parameter Q on the internal profile is depicted in figure 11. Most important of all, it illustrates the favourable effect a positive pressure gradient in an expansive pseudo-shock has on the boundary-layer flow. At the beginning of the

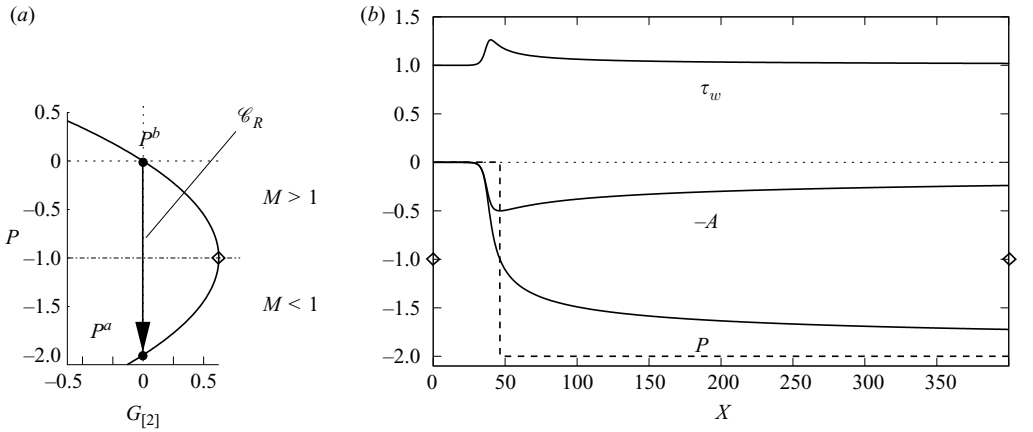

FIGURE 10. (*a*) Plot of the mass flux density $G_{[2]}$ for quadratic nonlinearity in the pressure and Rayleigh line connecting the pressure before and after the shock, P^b and P^a. (*b*) Plot of the perturbation of the pressure, displacement thickness and wall shear for $Q=1$, $S_{-\infty}=0$.

interaction process, the lower-deck flow passing the interaction region is accelerated rather than decelerated as in the classical compressive case treated in the previous section. As soon as the sonic state has been transversed in the upper-deck flow regime the lower-deck flow decelerates and approaches the undisturbed initial flow profile in the limit $X\to\infty$. Consequently, the distribution of the wall shear stress exhibits a local maximum which increases with the increasing steepness of the pressure profile. Also note that $\tau_w \geqslant 1$ in the entire interaction region, so that the flow remains firmly attached for all possible values of Q, quite in contrast with the case of compression pseudo-shocks.

5.5. *Sonic pseudo-shock*

As the third example, the internal profile of a sonic rarefaction shock is considered (cf. table 4 for the selected inflow conditions and scaled quantities and figure 6). A sonic shock is only possible in the case of mixed nonlinearity, that is to say if Γ changes sign in the considered flow regime, resulting in a non-convex flux function $G_{[3]}$ as is in figure 12(*a*). The admissible rarefaction shock in the situation under consideration results in a transition from a supersonic flow state to a sonic state, i.e. $M=1$. As before, the shock discontinuity in the pressure indicated by the dashed lines resolves into a smooth internal-shock profile connecting $P^b=0$ and $P^a=-4$. The algebraic decay of the pressure far downstream in case of a shock terminating in a sonic state, i.e. $G'_{[n]}(P^a)=0$, has been found to be even weaker than in the case of a shock terminating at a subsonic state, i.e. $G'_{[n]}(P^a)\neq 0$ (cf. § 4.3). The predicted weaker decay is confirmed by figure 13 which shows the excellent agreement of the leading-order term of the pressure distribution far downstream based on the analytical results (4.20) and (4.22) with the numerical solution. This weaker algebraic decay results in an increased length of the shock profile as can be seen by comparing e.g. figure 8 and figure 13.

Alternatively to a shock connecting supersonic flow upstream with sonic flow downstream considered so far, a sonic shock can equally well connect sonic flow upstream with subsonic flow downstream in accordance with the shock admissibility criteria, Theorem 3.1, since the condition $[M]<0$ is satisfied in the latter case just as well. Evaluation of the exponent (4.6) governing the exponential growth of the flow quantities far upstream (4.1) results in $\kappa=0$ because of $G'_{[3]}(P^b)=0$, meaning

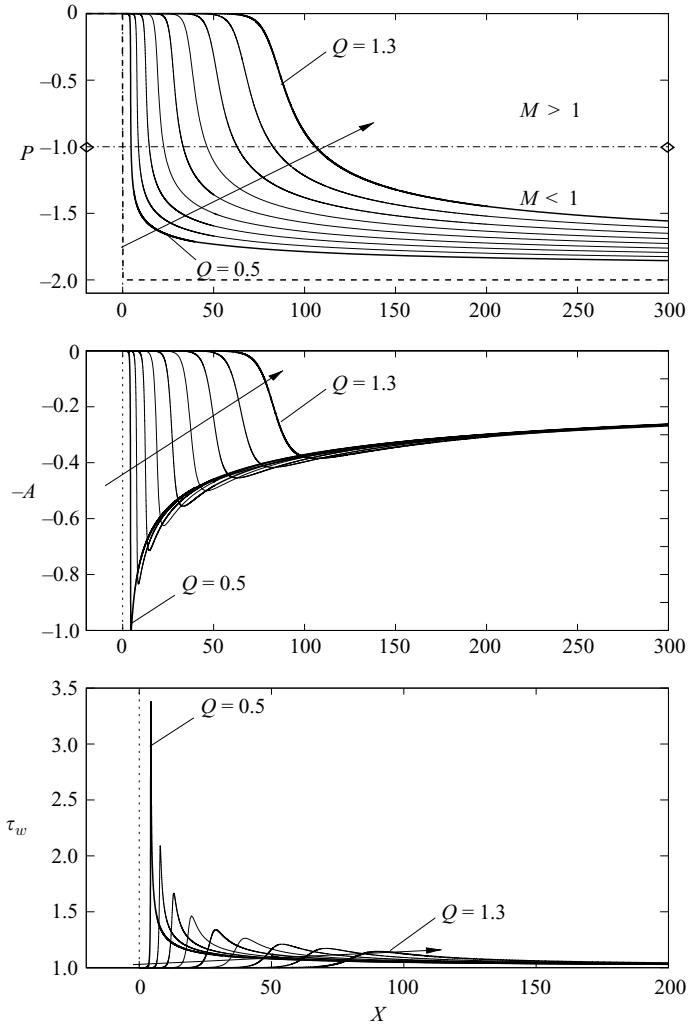

FIGURE 11. Distributions of the pressure, displacement thickness and wall shear stress in an internal-shock profile connecting P^b and P^a for various values of Q and $S_{-\infty} = 0$; $Q = 0.5, 0.6, \ldots, 1.3$.

that Lighthill's ansatz yields the trivial eigensolution in this case. On the other hand, there always exists a non-trivial eigensolution for each supersonic flow state upstream, no matter how close it is to the sonic flow state. Consequently, the internal-shock profile of a sonic shock originating in a sonic flow can be seen as the limiting case of internal-shock profiles originating in supersonic flow when $M^b \to 1^+$. This will be exemplified in more detail in the next section dealing with the internal-shock profile of a double-sonic shock.

5.6. *Double-sonic pseudo-shock*

The selected inflow conditions and scaled quantities used for the calculation of internal profiles of a double-sonic shock are summed up in table 4 and figure 6.

Similar to the case of a simple sonic shock a double-sonic shock is only possible in the case of mixed nonlinearity, if Γ changes its sign in the considered flow regime,

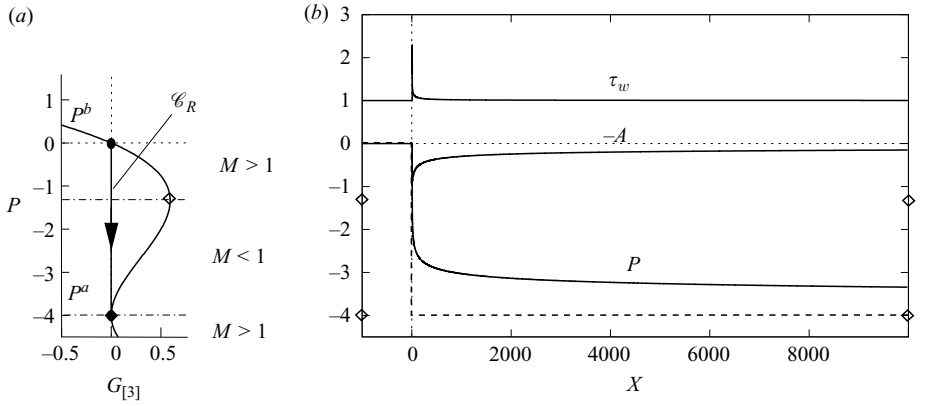

FIGURE 12. (*a*) Plot of the mass flux density $G_{[3]}$ for cubic nonlinearity in the pressure and Rayleigh line connecting the pressure before and after the shock, P^b and P^a. (*b*) Plot of the perturbation of the pressure, displacement thickness and wall shear for $Q = 1$, $S_{-\infty} = 0$.

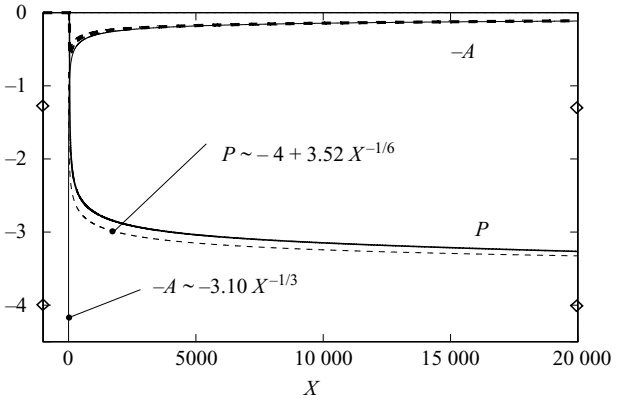

FIGURE 13. Plot of the pressure P and the displacement thickness $-A$ for $Q = 1$, $S_{-\infty} = 0$ and comparison of the asymptotic behaviour far downstream $X \gg 1$ predicted by (4.20) and (4.22).

resulting in a non-convex flux function (cf. figure 14*a*). Strictly speaking, a double-sonic shock forms only if Γ changes sign twice. This, however, results in a mass flux density $G_{[n]}$ which is a polynomial of fourth order in the pressure, i.e. the case $n = 4$ in (3.36). Referring to figure 6, the double-sonic shock originates in a thermodynamic region in the pressure-versus-density diagram close to the point at which an isentrope touches the transition line $\Gamma = 0$. Since the second derivative of Γ, i.e. N, has to be positive in the region of interest (cf. Kluwick 1993), the flux function $G_{[4]}$ always takes on a shape similar to the example depicted in figure 14 such that $G_{[4]}(P) \to +\infty$ for $P \to \pm\infty$ (see (3.36)). The internal-shock profile of a double-sonic shock is the limiting case of internal-shock profiles originating in supersonic flow when $M^b \to 1^+$ (cf. figure 14). As earlier, the pressure jump across a double-sonic shock is indicated by the dashed lines in the plot of the pressure distribution in figure 14(*b*). The flow conditions upstream of the interaction region are adjusted by varying the parameter $QS_{-\infty}$ in the interaction law, thus shifting the Rayleigh lines from right to left by a distance $-QS_{-\infty}$ from the origin (see figure 14*a*). The limiting case of a double-sonic shock is then obtained for $QS_{-\infty} = QS_{-\infty,max}$ (see figure 14). Prescribing a

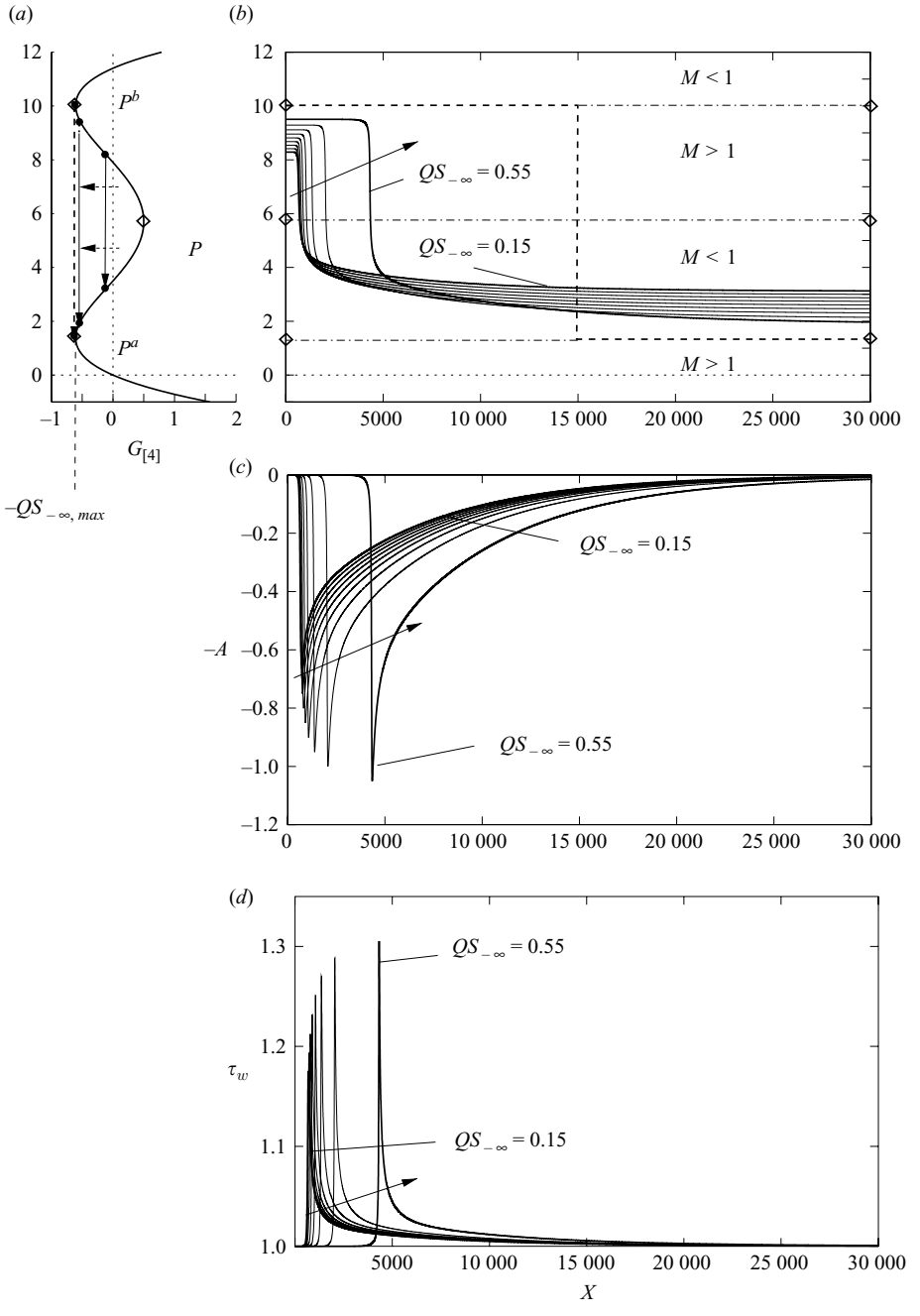

FIGURE 14. (*a*) Plot of pressure P versus the mass flux density $G_{[4]}$. The Rayleigh lines are shifted from right to left by varying $QS_{-\infty}$, successively approaching the limiting case of a double-sonic shock for $QS_{-\infty,max}$ indicated by the dashed Rayleigh line. Plots of the (*b*) induced pressure, (*c*) displacement thickness and (*d*) wall shear stress for $Q = 1$, $QS_{-\infty} = 0.15, 0.20, \ldots, 0.55$. In (*b*) a double-sonic shock for the case of inviscid flow indicated by the dashed lines is included for illustration.

value $QS_{-\infty} \neq 0$ is equivalent to changing the height of the channel and the inflow conditions according to (3.42).

Considering the various Rayleigh lines in figure 14 it is evident that the overall shock strength increases while approaching the limiting double-sonic shock. On the other hand, considering the plot of the internal pressure profiles, the length of the corresponding internal-shock profiles, i.e. the region of significant variation of the pressure, is increasing as well. This phenomenon of increasing shock thickness for increasing shock strength already has been reported in a different context by Cramer & Crickenberger (1991), who studied internal-shock profiles resulting from a classical thermo-viscous regularization.

Moreover, an admissible double-sonic shock is bound to be a rarefaction shock in accordance with the shock admissibility criteria for the inviscid case (Theorem 3.1). This can be concluded from inspection of figure 14, taking into account the arguments concerning the possible shapes of the flux function $G_{[4]}$ addressed at the beginning of this section. A double-sonic shock has to connect two separate extrema of $G_{[4]}$, and since $G_{[4]} \to \infty$ for $P \to \pm\infty$ because of $N > 0$, these two extrema have to be minima. The remaining extremum of $G_{[4]}$ is a maximum and has to lie in between. Let $P^1_{min} > P^2_{min}$ characterize the two separate minima and P_{max} the maximum. Then $G'_{[4]} < 0$ for $P \in \{P^1_{min}, P_{max}\}$ and $G'_{[4]} > 0$ for $P \in \{P_{max}, P^2_{min}\}$, and consequently, the internal-shock profiles used to construct the limiting solution of a double-sonic shock can correspond to rarefaction shocks only, and thus a double-sonic shock likewise has to be a rarefaction shock.

5.7. *Split pseudo-shock*

As the fifth and last example we consider the internal profile of a split shock; for the selected inflow conditions and scaled quantities, again consult table 4 and figure 6. Similar to the case of a double-sonic shock Γ has to change its sign twice in the considered flow regime, i.e. $n = 4$, resulting in a non-convex flux function which is represented by a polynomial of fourth order in the pressure (figure 15*a*). The Rayleigh line of the split shock is given by the dashed line which touches the flux function $G_{[4]}$ in a sonic point at the distance $QS_{-\infty,max}$ from the origin. As before, the split shock has to be interpreted as the limiting case of classical Lax shocks for $QS_{-\infty} \to QS_{-\infty,max}$. The flow in the upper-deck region has to pass through three sonic sates (cf. figure 15), while the overall shock leads to a transition from supersonic conditions to subsonic conditions. The three sonic states result in three extrema in the distribution of the displacement thickness $-A$. The lower-deck flow generates a viscous Laval nozzle which consists of two throats and one anti-throat in order to allow a smooth acceleration of the upper-deck flow through the different Mach number regimes. Taking a look at the calculated pressure distribution of internal-shock profiles for various values of $QS_{-\infty}$ on the right-hand side in figure 15 reveals that the phenomenon of shock splitting can already be anticipated from the pressure profiles for values of $QS_{-\infty} < QS_{-\infty,max}$. After the upper-deck flow has passed through the first sonic state resulting in a passage from supersonic flow to subsonic flow, the flow medium enters a plateau region while passing the second sonic state, as the flow is accelerated back to supersonic conditions. Finally, the then-supersonic flow passes the third sonic state, and the flow becomes subsonic again. The last transition from supersonic conditions to subsonic conditions results in a second steepening of the shock profile. This phenomenon of impending shock splitting becomes more and more pronounced, successively separating the two regions of rapid pressure rise for $QS_{-\infty} \to QS_{-\infty,max}$. From the existence of this limiting form of the internal-shock

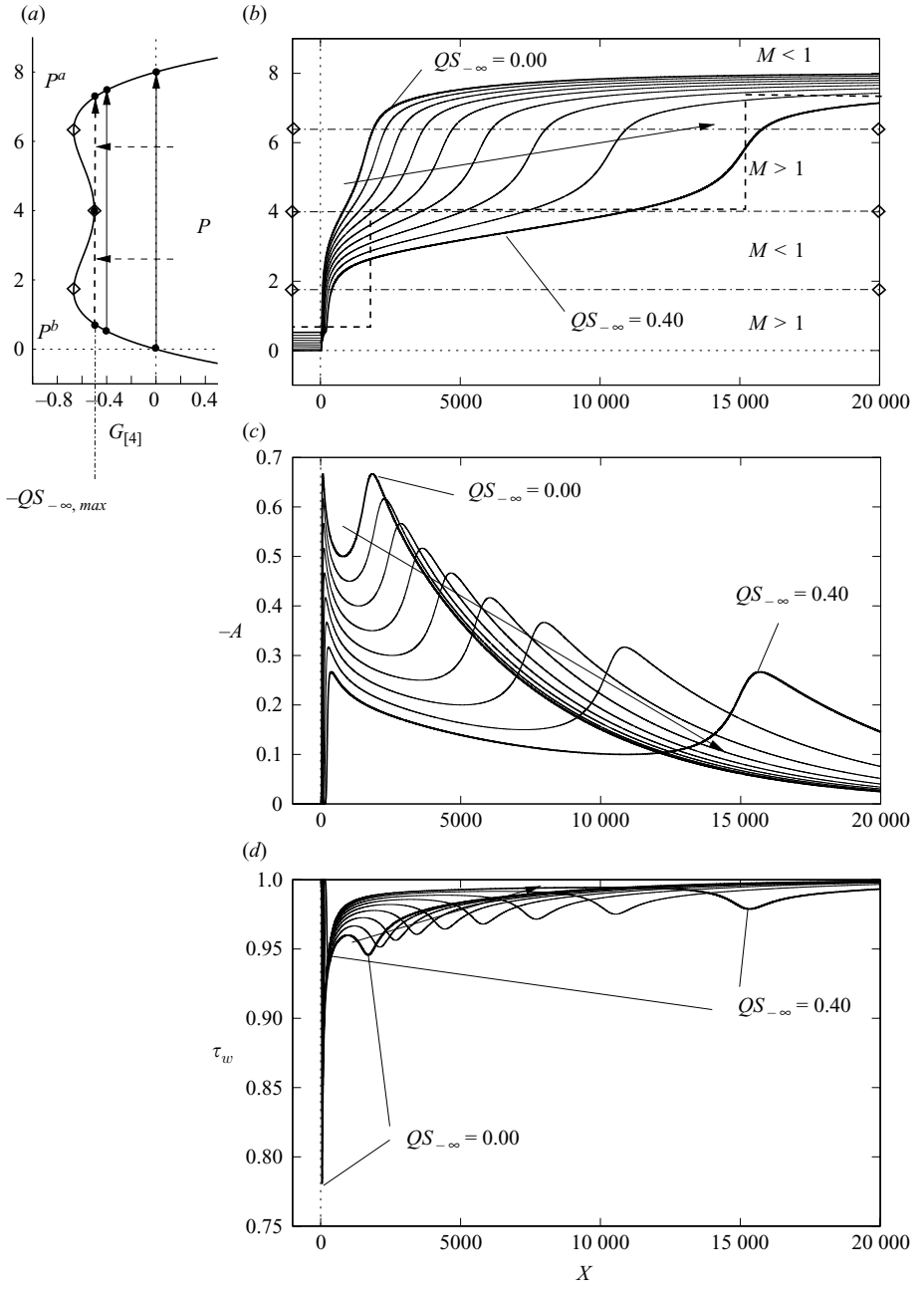

FIGURE 15. (*a*) Plot of pressure P versus the mass flux density $G_{[4]}$. The Rayleigh lines are shifted from right to left by varying $QS_{-\infty}$, successively approaching the limiting case of a split shock for $QS_{-\infty,max}$ indicated by the dashed Rayleigh line. Plots of the (*b*) induced pressure, (*c*) displacement thickness and (*d*) wall shear stress for $Q = 1$, $QS_{-\infty} = 0.00, 0.05, \ldots, 0.40$. In (*b*) a split shock for the inviscid case indicated by the dashed lines is included for illustration.

profile one infers that indeed two shocks forming a split shock may coexist next to each other in purely inviscid flow. Interestingly enough, similar to the case of a double-sonic shock discussed before, this phenomenon of impending shock splitting

has also been observed by Cramer & Crickenberger (1991), for internal-shock profiles resulting from a thermo-viscous regularization.

6. Summary and conclusions

In this treatise viscous–inviscid interactions in internal, transonic, single-phase and two-dimensional high-Reynolds-numbers flows through channels that are so narrow that the interacting core-region flow becomes one-dimensional to the leading order are shown to be described consistently by a triple-deck problem (cf. § 3). The interacting core region is hereby represented by a single upper deck which is shared by the two interacting boundary layers at the lower and upper channel walls. The resulting model equations then are applied to study the shock–boundary-layer interaction in a narrow channel of constant cross-section. It is demonstrated that a shock discontinuity is smoothed out by the interaction process, ultimately resulting in an internal-shock profile. Furthermore, internal shock profiles and pseudo-shocks are found to be identical in the context considered here. Both are represented by non-trivial eigensolutions to the interaction problem.

The mechanism of viscous–inviscid shock regularization which arises in the context of internal flows as considered here is governed by completely different underlying physics than the well-known mechanism leading to the Taylor shock profile known e.g. from studies of external flows. In the latter case the effects of viscous normal stresses and heat conduction are the essential ingredients of the regularization process which, however, are negligible in the type of internal flows considered here, where boundary layers generated because of the action of viscous shear stresses form a 'viscous' nozzle adapting to and at the same time interacting with the inviscid channel core flow and thus allow a smooth passage of the inviscid core-region flow through the interaction region. This mechanism is thoroughly discussed in the study of internal-shock profiles of various weak anomalous shocks forms possible in fluids of mixed nonlinearity (BZT fluids), i.e. rarefaction, sonic, double-sonic and split shocks (cf. §§ 4 and 5). It is found that possible internal-shock profiles are consistent with the shock admissibility criterion formulated for the inviscid case (cf. Kluwick 1993). Interestingly enough, the internal-shock profiles because of viscous–inviscid interactions share common features with those obtained by a classical thermo-viscous regularization, e.g. impending shock splitting.

The calculation of the characteristic length scales involved in the distinguished limit for a particular example BZT fluid, PP10 (cf. table 4), illustrates that such flow phenomena as discussed here can be encountered in internal flows of a BZT fluid in future engineering practice. However, besides the interesting features of BZT fluids, like the fact that the boundary-layer flow remains firmly attached to the wall under the influence of a rarefaction shock and thus a source of severe flow losses encountered in technical applications such as organic Rankine cycle processes could be avoided, an experimental proof of their existence is still lacking so far. The set-up described here could be an alternative to shock tubes currently in use to experimentally prove the existence of rarefaction shocks. The distinguishing advantages over a shock-tube experiment would be that the shock position is stationary and that no other wave phenomena would have to be accounted for. A disadvantage, however, may be the need to guarantee laminar boundary-layer flow up to very high Reynolds numbers and that the actual position at which a weak normal shock forms in a channel of constant cross-section is very sensible to small perturbations. Therefore, a theory of

viscous–inviscid interactions in narrow nozzles is of interest, which will be the focus of an forthcoming publication by the authors.

It shall be pointed out that the presented theory has been obtained by means of an asymptotic analysis, and consequently the quality of such an asymptotic theory relies on the smallness of an expansion parameter. What can be considered to be sufficiently small for a particular problem can only be accessed by experiments or by computational fluid dynamics simulation of the full problem in the end. However, we emphasize that asymptotic analysis is a means to isolate relevant physical effects, and the application of triple-deck theory to other important problems in boundary-layer theory has proven to be extremely successful in the past.

This work has been financed by the Austrian Science Fund in the framework of the WK Differential Equations.

REFERENCES

Abramowitz, M. & Stegun, I. A. 1970 *Handbook of Mathematical Functions*, 7th edn. Dover.

Anderson, D. A., Tannehill, J. C. & Pletcher, R. H. 1997 *Computational Fluid Mechanics and Heat Transfer*, 2nd edn. Taylor & Francis.

Bethe, H. A. 1942 The theory of shock waves for an arbitrary equation of state. *Report* 545. Office of Scientific Research & Development.

Chandrasekar, D. & Prasad, P. 1991 Transonic flow of a fluid with positive and negative nonlinearity through a nozzle. *Phys. Fluids* A **3** (3), 427–438.

Chung, T., Ajlan, M., Lee, L. L. & Starling, K. E. 1988 Generalized multiparameter correlation for nonpolar and polar fluid transport properties. *Indus. Engng Chem. Res.* **27**, 671–678.

Cinnella, P. & Congedo, P. M. 2007 Inviscid and viscous aerodynamics of dense gases. *J. Fluid Mech.* **580**, 179–217.

Colonna, P. & Guardone, A. 2006 Molecular interpretation of nonclassical gasdynamics of dense vapours under the van der Waals model. *Phys. Fluids* **18**, 056101.

Colonna, P., Guardone, A. & Nannan, N. R. 2007 Siloxanes: a new class of candidate Bethe–Zel'dovich–Thompson fluids. *Phys. Fluids* **19**, 086102.

Colonna, P. & Silva, P. 2003 Dense gas thermodynamic properties of single and multicomponent fluids for fluid dynamics simulations. *J. Fluids Engng* **125**, 414–427.

Cramer, M. & Kluwick, A. 1984 On the propagation of waves exhibiting both positive and negative nonlinearity. *J. Fluid Mech.* **142**, 9–37.

Cramer, M. S. 1989 Negative nonlinearity in selected fluorocarbons. *Phys. Fluids* A **1** (11), 1894–1897.

Cramer, M. S. 1991 Nonclassical dynamics of classical gases. In *Nonlinear Waves in Real Fluids*, CISM Courses and Lectures No. 315 (ed. A. Kluwick), pp. 91–145. Springer Wien.

Cramer, M. S. & Crickenberger, A. B. 1991 The dissipative structure of shock waves in dense gases. *J. Fluid Mech.* **223**, 325–355.

Cramer, M. S. & Sen, R. 1986 Exact solutions for sonic shocks in van der Waals gases. *Phys. Fluids* **30** (2), 377–385.

Fergason, S. H., Ho, T. L., Argrow, B. M. & Emanuel, G. 2001 Theory for producing a single-phase shock wave. *J. Fluid Mech.* **445**, 37–54.

Gittler, Ph. 1992 On similarity solutions occurring in the theory of interactive laminar boundary layers. *J. Fluid Mech.* **244**, 131–147.

Guardone, A. & Argrow, B. M. 2005 Nonclassical gasdynamic region of selected fluorocarbons. *Phys. Fluids* **17**, 116102.

Kluwick, A. 1993 Transonic nozzle flow of dense gases. *J. Fluid Mech.* **247**, 661–688.

Kluwick, A. 1994 Interacting laminar boundary layers of dense gases. *Acta Mech.* **4** (Suppl.), 335–349.

Kluwick, A. 1998 Interacting laminar and turbulent boundary layers. In *Recent Advances in Boundary Layer Theory*, CISM Courses and Lectures No. 390 (ed. A. Kluwick), pp. 231–330. Springer Wien.

Kluwick, A. 2004 Internal flows of dense gases. *Acta Mech.* **196**, 123–143.

Kluwick, A. & Bodonyi, R. J. 1979 Freely interacting laminar boundary layers in channels. *ZAMM* **59**, T243–T245.

Kluwick, A., Exner, A., Cox, E. A. & Grinschgl, Ch. 2009 On the internal structure of weakly nonlinear bores in laminar high Reynolds number flow. *Acta Mech.* doi:10.1007/s00707-009-0188-x.

Kluwick, A. & Scheichl, St. 1996 Unsteady transonic nozzle flow in dense gases. *J. Fluid Mech.* **310**, 113–137.

Kluwick, A., Scheichl, S. & Cox, E. A. 2007 Near-critical hydraulic flows in two-layer fluids. *J. Fluid Mech.* **575**, 187–219.

Lighthill, M. J. 1953 On boundary layers and upstream influence. Part II. Supersonic flows without separation. *Proc. R. Soc.* A **217**, 478–504.

Martin, J. J. & Hou, Y. 1955 Development of an equation of state for gases. *AIChE J.* **1** (2), 142–151.

Matsuo, K., Miyazato, Y. & Kim, H. 1999 Shock train and pseudo-shock phenomena in internal gas flows. *Progr. Aerosp. Sci.* **35** (1), 33–100.

Menikoff, M. & Plohr, B. J. 1989 The Riemann problem for fluid flow of real materials. *Rev. Mod. Phys.* **61** (1), 75–130.

Oleinik, O. A. 1957 Discontinuous solutions of nonlinear differential equations. *Am. Math. Soc. Trans.* **26**, 95–172.

Reyhner, T. A. & Flügge-Lotz, I. 1968 Interaction of a shock wave with a laminar boundary layer. *Intl J. Nonlin. Mech.* **3**, 173–199.

Stewartson, K. 1974 Multistructured boundary layers on flat plates and related bodies. *Adv. Appl. Mech.* **14**, 145–239.

Stewartson, K. & Williams, P. G. 1969 Self-induced separation. *Proc. R. Soc.* A **312**, 181–206.

Thompson, P. A. 1971 A fundamental derivative in gasdynamics. *Phys. Fluids* **14**, 1843–1849

Thompson, P. A., Chaves, H., Meier, G. E. A., Kim, Y. & Speckmann, H.-D. 1987 Wave splitting in a fluid of large heat capacity. *J. Fluid Mech.* **185**, 385–414.

Thompson, P. A. & Lambrakis, K. C. 1973 Negative shock waves. *J. Fluid Mech.* **60** (1), 187—208.

Zamfirescu, C., Guardone, A. & Colonna, P. 2008 Admissibility region for rarefaction shock waves in dense gases. *J. Fluid Mech.* **599**, 363–381.

Zel'dovich, Y. B. 1946 On the possibility of rarefaction shock waves. *Zh. Eksp. Teoret. Fiz.* **4**, 363–364.